machines

MDPI

Article

Analytical Model of Tapered Thread Made by Turning from Different Machinability Workpieces

Oleh Onysko [1,*], Volodymyr Kopei [1], Cristian Barz [2], Yaroslav Kusyi [3], Saulius Baskutis [4], Michal Bembenek [5], Predrag Dašić [6] and Vitalii Panchuk [1]

1 Department of Computerized Mechanical Engineering, Ivano-Frankivsk National Technical University of Oil and Gas, Karpatska Str., No. 15, 76019 Ivano-Frankivsk, Ukraine; volodymyr.kopey@nung.edu.ua (V.K.); vitalii.panchuk@nung.edu.ua (V.P.)
2 North University Centre of Baia Mare, Technical University of Cluj-Napoca, Victor Babes Str., No. 62A, 430083 Baia Mare, Romania; cristian.barz@ieec.utcluj.ro
3 Department of Mechanical Engineering and Transport, Lviv Polytechnic National University, Stepan Bandera Str., No. 12, 79013 Lviv, Ukraine; jarkym@ukr.net
4 Department of Production Engineering, Kaunas University of Technology, 56, Studentu Str., 51424 Kaunas, Lithuania; saulius.baskutis@ktu.lt
5 Department of Manufacturing Systems, Faculty of Mechanical Engineering and Robotics, AGH University of Krakow, 30 Mickiewicza Avenue, 30-059 Krakow, Poland; bembenek@agh.edu.pl
6 Engineering Academy of Serbia (IAS), Str. Kneza Miloša 9/IV, 11000 Belgrade, Serbia; dasicp58@gmail.com
* Correspondence: oleh.onysko@nung.edu.ua

Abstract: High-precision tapered threads are widely used in hard-loaded mechanical joints, especially in the aggressive environment of the drilling of oil and gas wells. Therefore, they must be made of workable materials often difficult to machine. This requires the use of high-performance cutting tools, which means the application of non-zero geometric parameters: rake and edge inclination angles. This study is based on analytical geometry methodology and describes the theoretical function of the thread profile as convoluted surfaces dependent on the tool's geometric angles. The experiments were conducted using a visual algorithm grounded on the obtained function and prove the practical use of the scientific result. They predict the required accuracy of thread made using a lathe tool with a rake angle of up to 12°.

Keywords: cutting-edge inclination angle; lathe tool rake angle; lead screw angle; convoluted helicoid; oblique helicoid; generator of ruled helicoid

Citation: Onysko, O.; Kopei, V.; Barz, C.; Kusyi, Y.; Baskutis, S.; Bembenek, M.; Dašić, P.; Panchuk, V. Analytical Model of Tapered Thread Made by Turning from Different Machinability Workpieces. *Machines* **2024**, *12*, 313. https://doi.org/10.3390/machines12050313

Academic Editor: Kai Cheng

Received: 20 March 2024
Revised: 22 April 2024
Accepted: 26 April 2024
Published: 3 May 2024

1. Introduction

Today, oil and gas well drilling is a key process in a number of applied industries that play a strategic role in guaranteeing economic stability [1,2]. In particular, this includes exploration and extraction of hydrocarbons and geothermal and mineral resources, environmental monitoring and scientific research of the subsoil, underground archaeological excavations, infrastructure development of large cities, etc. [3]. The threaded connections of a drill string have to withstand huge axial tension, severe working torque, and extreme bending. When these loads exceed a certain value, threaded connections often fail, causing enormous losses [4]. There are no formulas for calculating the torsional capacity of threaded connections under complex loads, even by API standards. To solve those challenges, the required values of the tensile strength of different steel groups for drill pipes are established by standards [5,6] (Table 1).

Table 1. Mechanical property grades of steel groups for oil and gas well drill pipes according to ISO [5] and GOST [6] standards.

Name of Property, Unit	Values of Mechanical Properties due to Strength Groups of Steel					
	D	E	X	G	S	Y (GOST Only)
Tensile strength σ, MPa	655	689	724	793	1000	1241
Flow stress σ_f, MPa (min)	379	517	655	724	931	1170
Flow stress σ_f, MPa (max)	-	724	862	931	1138	-

We must take into account that group S and, in particular, group Y are difficult-to-machine materials. Reference [6] presented Y as a prospective steel more than 30 years ago, and it looks like a future material even today. There are studies that investigate the possibility of improving the quality of tool-joint thread manufactured from light alloy [7]. Further, there are special studies about drilling and casing strings, as well as pipelines, which are complex, elongated elastic mechanical systems comprising metallic and non-metallic materials with many threaded connections [8,9]. Threaded connections are used to maintain the structural integrity and tightness of pipe columns in wells and pipelines, so the quality of their materials [10,11] and the reliability of their structure are subject to increased requirements [12].

A key advantage of threaded connections compared to other methods of connecting pipes and tools in the drill string is that they can be disassembled and reused many times. At the same time, this advantage can become a source of problems for the entire structure due to unintentional self-unscrewing of the threaded connection [13–16].

In most cases, threaded connections for drill string elements work in aggressive and abrasive environments under the influence of intense dynamic and long-term cyclic loads [17,18]. The increase in drilling depths and the construction of wells with complex spatial configurations require the use of modern materials [19,20], intelligent structures, and advanced technologies for designing and manufacturing drill tool joints [21–23].

Therefore, it seems that engineers and scientists have two yet-unsolved tasks: the first, obtaining special algorithms of stress analysis, models and techniques to strengthen the drill string, and second, providing special conditions for producing a hard and durable tool-joint thread.

The stress state of pipes and cylindrical shells near sharp-end concentrators under the conditions of contact interaction was studied in papers [24,25]. Certain works [26] explain the effect of the closure of collinear cracks on the stress–strain state and the limiting equilibrium of bent shallow shells that are similar to the thread of the screw. Those studies are too theoretically deep and cannot be used easily.

The modeling of thread based on analytical data can be found in articles specializing in screw investigation. In reference [27], computer modeling of the dynamic processes in the example of the transverse vibration of the thread during operation has been proposed. The research is based on the differential theory of vibration methodology. Article [28] presents bolt-joint research on the torque–force relationship both for the theoretical analyses and the experimental results. Theoretical modeling and simulation of the complex helical surfaces of threads and their accuracy related to machining conditions provide useful information for predicting real process accuracy but for whirled lead screws only [29]. Reference [30] applies an approach that is based on analytical equations describing thread surfaces that necessarily fall into the class of Bonnet surfaces. Each of the presented papers uses local theory analysis, which cannot be applied to all types of screw thread.

Machinability and mechanical properties of materials for parts and thread connectors, in particular, must be estimated before their manufacturing. Paper [31] analyzes the influence of the mechanical properties of different materials of weighted drill pipes on the value of free-force clamping force in thread connectors. In reference [32], the effects of cutting parameters on the turning characteristics of AISI 52100 hard-to-machine steel are

investigated. An experimental study was conducted for evaluation regarding cutting force and chip shape, tool flank wear, and surface roughness.

The research presented in [33] shows the complexity of the machining of the rope threads mainly focusing on tool kinematics as a function of cutting parameters and tool geometry. The paper [34] reviews the recent progress in the non-traditional energy-assisted mechanical machining of difficult-to-cut materials for aircraft, mainly focusing on laser, electric, magnetic, chemical, and advanced processes.

The paper [35] provides experimental evidence of a cutting-edge geometric effect on the cutting forces in the workpiece. Only a tool with a non-zero rake angle can produce correct cutting conditions.

The technology of manufacturing helical and toothed surfaces requires an analytical approach to their shaping [36], the optimization of the technological route [37,38], the study of the latest approaches to stabilization of turning processes [39], and the development of special designs of cutting tools to ensure their shaping with minimal errors [40,41]. As presented by [42], the thread screw wear prediction method explains that reducing the ambient temperature is beneficial for enhancing the wear resistance of the screw. A thread milling motion control experiment realized with the help of a testbench validated that the method of PMSM driving developed in [43] significantly reduces contour errors compared with the usual methods. The paper [44] shows the results of the comparison of different coatings for high-speed steel threading. A control system for assessing thread quality in high-speed tapping using the signal of the spindle motor torque is developed in [45]. The article [46] studies the on-machine measurement method of screw threads of sucker rods based on machine vision. The investigation [47] shows that the lubrication method is the most important factor that affects thread precision. The paper [48] shows research on thread milling cutting forces for drill-string connection. The aim of the paper [49] is to ensure fast and accurate detection using the intelligent tapping process but not turning.

Turning is the most useable and main process in modern thread manufacturing of large-pitch screws and pipes of big diameter. The paper [50] describes the relationship between vibration and tool wear at the time of threading using a lathe. The work [51] formulates the generalized dynamics of thread-turning operations with custom multipoint inserts. The mechanism of closed-loop chip formation is modeled by evaluating the effect of the process vibrations. In the investigation [52], the deviations during lathe threading caused by mechanical deformations are provided and calculated. The study [53] presents a generalized and new systematic approach to predict the cutting forces in thread turning. The thread turning of aluminum alloy has been studied in [54]. The surface quality of thread flank faces was improved by using micro-hole textured solid-lubricant embedded carbide inserts. The paper [55] formulates the generalized dynamics of thread-turning operations with custom multipoint inserts. The mechanism of closed-loop chip formation is modeled by evaluating the effect of the process vibrations. The study [56] examined the influence of such factors as cutting speed and turning direction on the quality of external thread surface made by turning on Inconel 718 shafts. The work [33] describes the kinematic analysis of turning a noncircular cross-section workpiece, using mathematical parameters to optimize the efficiency of the process.

The optimization of high-performance cutting modes in the manufacture of threads requires an analysis of tool wear and the nature of changes in the roughness and accuracy of the thread, as well as the development of new methods of thread formation [57]. The optimization proposed by the study [58] presents an increase of about 5 HV0.2 in the hardness of the thread surface. The results presented in [59] guide the optimization of microtube threading simulation development and design to reduce cost and increase product quality. On the basis of 2^5 multifactorial experiments, a mathematical model of the influence of the parameters of the threading process on the parameters of the screw and its surface accuracy was obtained in [29].

Vibration-assisted machining and laser-assisted machining involve inducing material modification to enhance machinability. These methods were studied in [34], but there

was no investigation of tool geometric parameters' influence on machinability during the turning of screw thread.

The effect of the rake angle on the thread accuracy during turning is explained in manuscripts [60,61]. There are few works containing the study of the influence of other tool geometric parameters on thread profile accuracy [22,62], but there are not any studies presenting the mutual influence of all main tool geometric parameters on the accuracy of thread. However, the correct choice of the geometry of the cutting edge can significantly increase the threading possibility of processing difficult-to-machine workpieces, increase the stability of the tool, and speed up the process of thread production.

The purpose of this study is to establish a theoretic model for ensuring the accuracy of forming a thread with a given triangular profile, functionally depending on its pitch, diameter, and all influencing geometric parameters of the turning tool that performs it, using an analytical method.

Section 1 of the paper illustrates the importance of the research; Section 2 outlines the contemporary theoretical principles regarding ensuring the precision of thread manufacturing; Section 3 illustrates the validation of the mathematical model for a tapered thread profile based on the geometric parameters of the cutter utilized; Section 4 displays the findings of the investigation acquired through the algorithm developed from the mathematical model; Section 5 presents the study's conclusions.

2. Materials and Methods

2.1. Modern Approaches for Choosing Materials for Hard-Loaded Screw Threads

Drill pipe joints (also known as tool joints) are large-pitch threaded male–female conical joints (nipple-coupling) with a diameter of 30 mm to 200 mm and a triangular profile (Figure 1). One of the requirements for the accuracy of a drill-string tool-joint thread is the accuracy of its half-profile angle α, which according to the standard [63] is the same for all its standard sizes and is $30 \pm 0.75°$ (Figure 1).

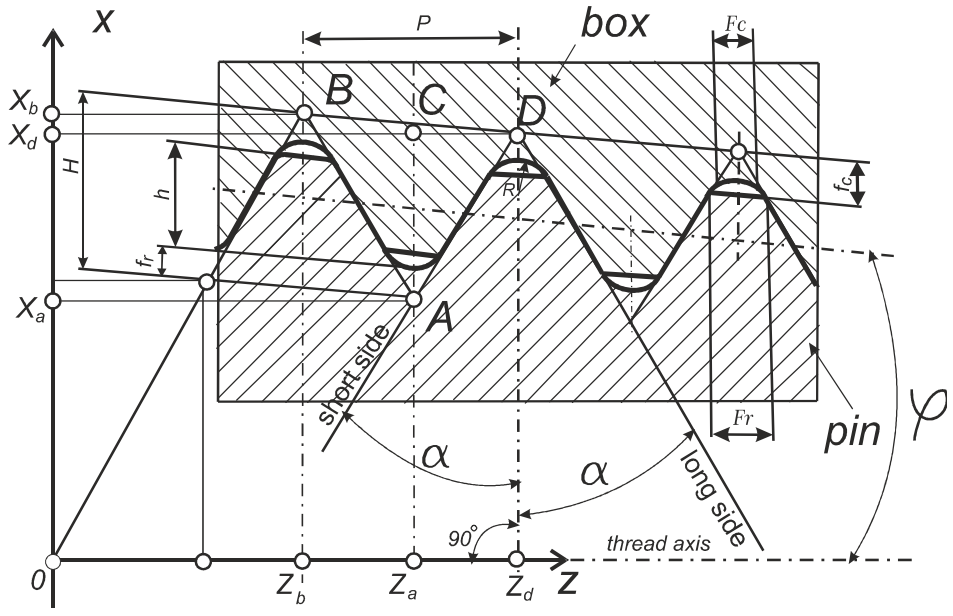

Figure 1. Scheme of a drill-string threaded connection according to the API7 standard with reference to the *ZOX* rectangular coordinate system: *H*—thread height (not truncated); *h*—thread height (truncated); *fr*—root truncation; *fc*—crest truncation; *R*—root radius; *P*—pitch.

There are a lot of screw threads with similar triangle profiles in general usage for all segments of engineering industry, including V-profile 60°, V-profile 60°, and ISO ($2\alpha = 60°$), and for pipe fittings and threads, including Whitworth ($2\alpha = 55°$), NPT Taper 1:16 ($2\alpha = 60°$), BSPT Taper 1:16 ($\alpha = 27.5°$), Aerospace threads ($2\alpha = 60°$) [63]. Only the taper API tool-joint

thread has a large pitch from 4.233 mm to 6.35 mm, and it is produced by mainly using a lathe [64].

Drill-string thread connectors (with API tool-joint tapered thread) are made using lathes, and thread cutters are used to turn their threaded surfaces. Modern manufacturers recommend using cutting tools with a full profile, which is similar to the profile and pitch P of one of the standard sizes of threading the tool joint [64]. At the same time, tool manufacturers offer a variety of materials and coatings for cutting inserts and recommend different tool feeding schemes for achieving better productivity or stability of the cutter. In scientific papers [65,66], methods of cutting in the process of thread turning from hard-to-machine AISI 304L stainless steels are investigated in order to reach a high stability of the cutter.

Simultaneously, the geometry of the rake surface of the cutter is never regulated by manufacturers; that is, the rake angle is actually always equal to 0. The zero-value rake angle of the cutters offered by the manufacturers is obviously related to compliance with the precision of the drill-string tool-joint thread regulated by the standard [63]. Despite the established approach of manufacturers, there are scientific studies that indicate the feasibility of using a non-zero value of the rake angle γ for turning in general and for turning oil and gas conical threads, in particular, threads made of high-alloy steel with a content of 13% Cr [67] and 3% Cr [68] (Figure 2).

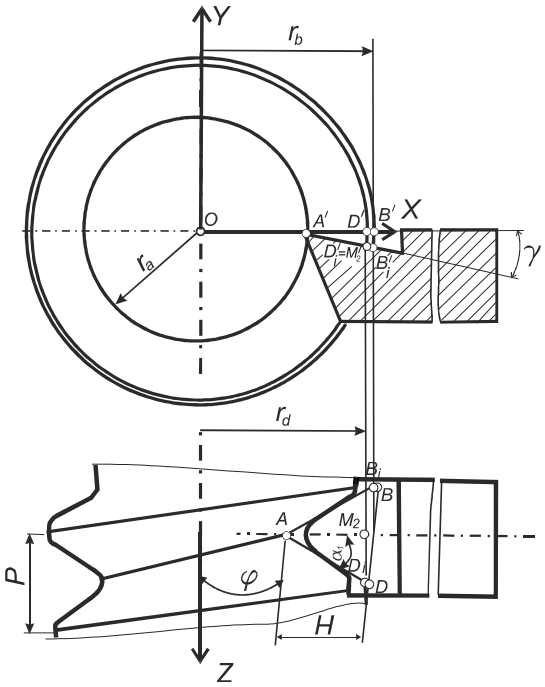

Figure 2. Scheme of installing a threaded cutter with a non-zero value of the rake angle ($\gamma > 0$).

Different alloy steels are used in drill-string thread connectors and other screws very often, especially if a corrosion environment in a well is predicted or a high strength level is needed. The machinability of that grade of steel varies from difficult to machine (range 1) to highly difficult to machine (range 3). ISO divides all steels into two big groups: carbon and alloy steels (group P) and stainless steel (group M). Workpiece Material Group presents subdivisions P1-P3 with an additional index, where an index value of 3 corresponds to the most difficult to machine, for example, P3.3 [69]. Materials AISI 4145H and GOST 35X3HMA belong to the category P3.3 (Table 2). The paper [68] established a rake angle of $-7°$ for one member of this category. Sandvik Coromant suggests its corporative MC (Material Classification) codes; for instance, P5.0.Z.PH is equal to M.3.3 [64]. AISI 416 stainless steel belongs to category P5.0.Z.PH for which the specific cutting force kc1 = 2800 (N/mm^2) is too large.

This material was investigated for threading in paper [67] with the recommendation of rake angle $\gamma = +12^\circ$ (Table 2).

Table 2. Machinability of materials used in automotive production, petrochemical, and drill-string pipes.

Group of Machine Parts	Grade of Steel	Machinability Range MC Code/WMG	Rake Angle	Reference
Pump shafts, marine applications, petrochemical industries	AISI 630 stainless steel DIN X5CrNiCuNb16-4 EN 1.4542	P5.0.Z.PH M3.3 2800 N/mm^2	-	[70]
Automotive part production, machine industry	AISI 416 stainless steel DIN X12CrS13	P5.0.Z.PH 2800 N/mm^2	+12°	[67,71]
Machine parts in corrosion environment	AISI 304L stainless steel DIN X5CrNi18-10	M3.1 M1.1.Z.AQ 2000 N/mm^2	-	[66]
Heavy-weight drill pipes, bolts, gears	AISI 4145 H 46MoMnCr01 low-alloy steel	P3.3	-	[72]
Drill pipes provide superior corrosion resistance at high temperatures	JFE-UHP^{TM} −15CR-125 (Japan) 0.03C-15Cr-6Ni-2Mo-1Cu stainless steel	M2.3	-	[73]
Heavy-weight drill pipes	GOST 35X3HMA high-alloy steel	P3.3	−7°	[68]
Drill-string pipes and tool joints	high-strength low-alloy steels		−5°	[61]

2.2. Geometrical Explanation of Manufactured Screw Thread as Convolute Helicoid Surface

The zero-value rake angle of the cutters offered by the manufacturers is obviously related to compliance with the precision of the drill-string tool-joint thread regulated by the standard [63].

Theoretical studies of the kinematics of the process of turning tapered thread using a tool with a non-zero value of the rake angle are presented in studies [60,74]. However, the scientific results in these papers concern the analytical calculations of the accuracy of the kinematics of turning the thread [74] and its predicted lead angle [60], and not its profile. Experimental studies of the influence of the error of setting the threaded cutter on the deviation of the real profile of the thread were carried out in [75]. The input data in this study are the tangential deviation of the cutter installation relative to the axis of the thread, as well as the angular displacement relative to the longitudinal axis of the tool. An analytical study of the effect of tool kinematics on the profile of the screw was carried out by the authors [76], but the object of the study is a cylindrical worm screw, and the subject is the profile and kinematics of the end mill, not the geometric angular parameters of its cutting edge. The paper [77] contains analytical dependence of the tool profile depending on its rake angle, but the tool is intended for the manufacture of a roller-gear cam and not a conventional worm (screw) shaft.

In cutters with a non-zero rake angle, the rectilinear section of the cutting edge of the tool does not cross the axis of the thread (Figure 2). In this scenario, due to the helical motion of the straight L, which corresponds to the straight AD where the straight section of the cutting edge is situated, a surface topology other than that prescribed by the standard is formed; i.e., instead of the Archimedean helicoid (Figure 3), a convoluted helicoid (Figure 4) is formed.

As it is known, helices are the guides of screws, so the drawings in Figures 3 and 4 show the inner helix h_2, on which the points of the inner radius of the thread r_a are theoretically located, and the outer helix h_3, on which the points of the outer radius of the thread r_d are theoretically located. The axis of screws i corresponds to the thread axis Z in Figure 2.

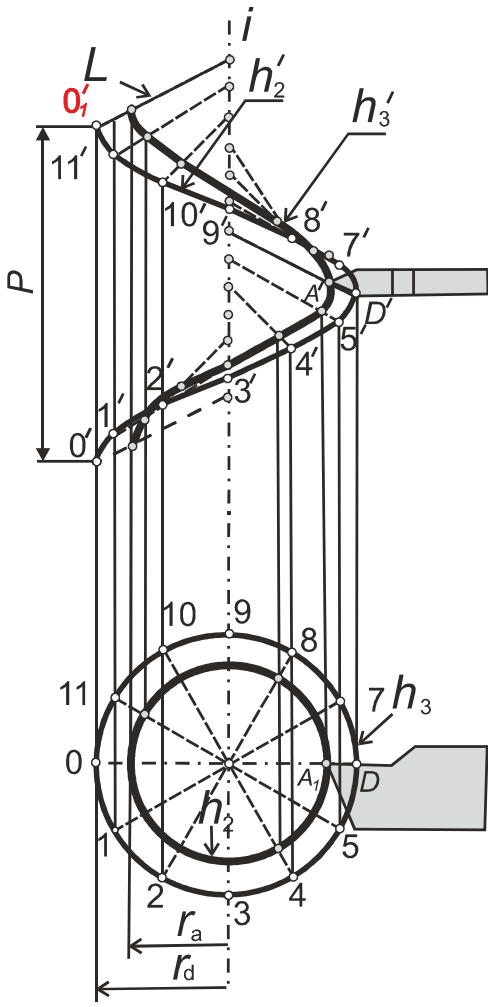

Figure 3. Scheme of execution of an oblique closed helicoid using a lathe cutter.

Additional characteristics for a convolute screw are as follows: an output cylinder with a radius r_1 and a helix h_1 on it (Figure 4).

Analogous constructions apply to and can be performed for another perpendicular section of the cut, located on the line AB, which is shown in Figure 2.

Based on the data of the draftsman of the standard [63], the starting point for designing the profile of the cutter is the Archimedean spiral surface, since the left AD and right AB of its lateral sides of its profile are rectilinear and such a cut is called triangular. Therefore, the axial profile of this surface is described by the equation with an algebraic linear function (Figure 1)

$$z = tan(\alpha)x, \tag{1}$$

where the angle $\alpha = 30°$ is the half-profile angle of the triangular thread.

To determine the theoretical profile of a cut formed by a cutter, the cutting edge of which does not lie in its axial section, it is necessary to have an analytical dependence of the axial section of the convolute helicoid on the value of the rake angle γ at the tool nose and the thread diameter, and to carry out its analytical comparison with the profile in the formula of the given thread (1).

Since the thread is conical, the variable nature of the values r_a, r_b, and r_1 should be taken into account in the calculations

$$\begin{aligned} r_a &= r_{amin} \cdot l \cdot cos(\varphi), \\ r_b &= r_{bmin} \cdot l \cdot cos(\varphi), \\ r_1 &= r_{1min} \cdot l \cdot cos(\varphi), \end{aligned} \tag{2}$$

where r_{amin}, r_{bmin}, and r_{1min} are minimum values of radii r_a, r_b, and r_1; l is the distance from the beginning of the screw thread with the small cone base to a certain turn of it.

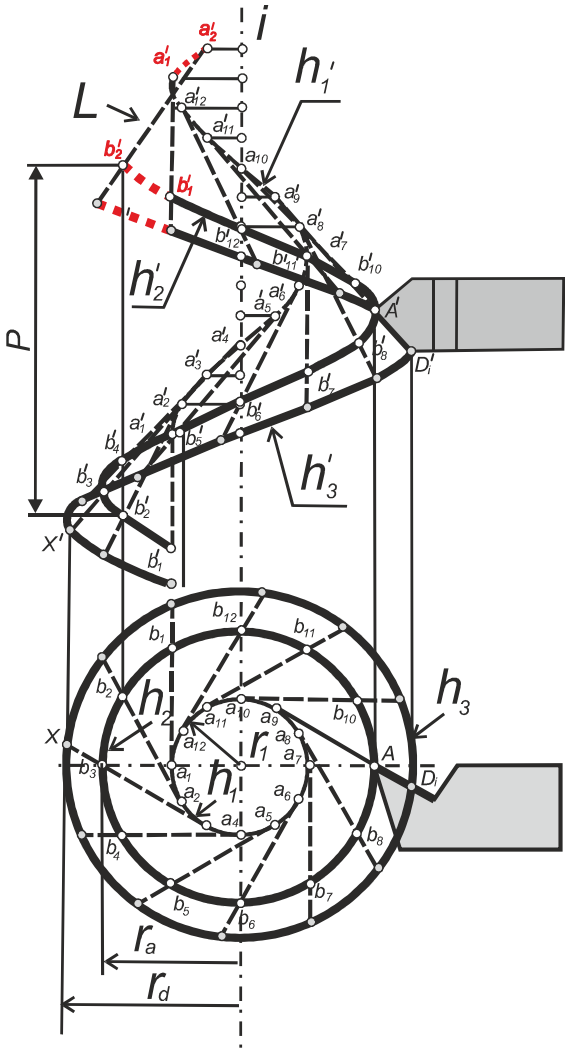

Figure 4. Scheme of execution of a convolute helicoid using a lathe cutter.

2.3. Analytical Method of Screw Thread Model Using Tool Back-Rake Parameter

In Figure 5, the generator L of the convoluted helicoid is constructed in cylindrical coordinates and at the same time in Cartesian coordinates. The XY plane is perpendicular to the Z-axis, which coincides with the thread axis and contains the starting point of coordinates O. Cylindrical coordinates are the most suitable for modeling the process of forming a helical surface with a turning tool.

The generator L of the convolute screw intersects the X-axis at point A, and it is inclined to the $X0Y$ plane at an angle α_1 (Figure 5). In the case of using a conventional cutting tool, the profile angles of the thread and the cutter are identical; i.e., $\alpha_1 = \alpha$. The projection of the generating L onto the coordinate plane $X0Y$ is the straight line M_1M_2. The segment AD_i lies on the generating L and is the cutting edge of the cutter. The plane defined by the triangle AD_iM_2 is the rake plane of the thread lathe tool. At the same time, the segment AD_iM_2 is parallel to the Z-axis, and its length, $|D_iM_2|$, determines the Z-coordinate of point D. The segment AM_2 is the projection of the cutting edge AD_i on the $X0Y$ plane. Point M_1 is the point of contact of the straight line M_1M_2 with the initial cylinder with radius r_1 [61].

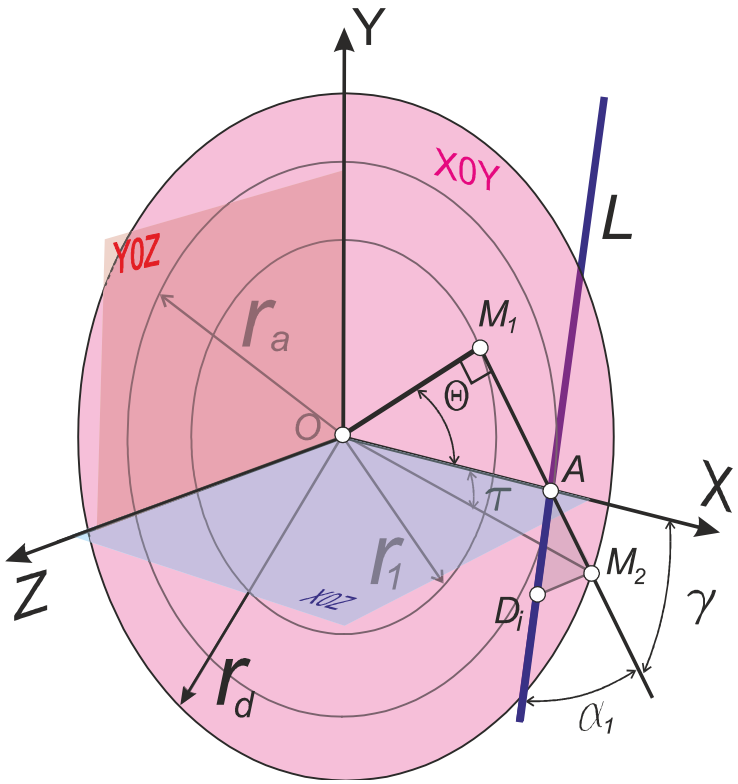

Figure 5. Schematic of the rake surface placement of the thread cutter in cylindrical coordinates.

2.3.1. Parametric Equations of the Helical Surface and Equations of Its Axial Section in General Form

If the generatrix L is set by a system of equations in cylindrical coordinates,

$$\begin{cases} \rho = f(\tau), \\ Z = F(\tau), \end{cases} \tag{3}$$

where the projection of L onto the $X0Y$ plane (line M_1M_2) is defined in polar coordinates by the equation

$$\rho = f(\tau), \tag{4}$$

where ρ is the distance of an arbitrary point of segment AM_2 to point O, then the helical surface is written in the following system of equations:

$$\begin{cases} X = f(\tau)cos(\tau + \theta), \\ Y = f(\tau)sin(\tau + \theta), \\ Z = F(\tau) + p\theta, \end{cases} \tag{5}$$

where the following definitions hold:

— Parameters τ and θ determine the position of a point on the surface and are its curvilinear coordinates. At the same time, the parameter τ determines the position of an arbitrary point of the line M_1M_2 on the projection of the generating line L on the $X0Y$ plane. The parameter θ determines the amount of rotation of the generator L around the Z-axis.

— The value p is a parameter of the screw and is determined by the formula

$$p = \frac{P}{2\pi},$$

where P is the pitch of the helicoid.

If we solve the Equation (4) with respect to the parameter τ:

$$\tau = f_1(\rho), \tag{6}$$

then the system of Equation (3) of the generatrix L in cylindrical coordinates will take the following form:

$$\begin{cases} \tau = f_1(\rho), \\ z = F_1(\rho), \end{cases} \tag{7}$$

where $F_1(\rho)$ denotes a certain complex function:

$$F(f_1(\rho)) = F_1(\rho).$$

Thus, the system of Equation (5) of the helical surface will have the following form:

$$\begin{cases} X = \rho cos(\tau + \theta), \\ Y = \rho sin(\tau + \theta), \\ Z = F_1(\rho) + p\theta, \end{cases} \tag{8}$$

where the parameter τ must be replaced by Formula (6). The coordinate lines are as follows: at θ = *const* is the generating line L, and at τ = *const* is the spiral line, which is placed on a cylinder with a radius of ρ.

Let us bring the system of Equation (8) to new curvilinear coordinates by making a substitution:

$$\varphi = \tau + \Theta.$$

The system of equations of the helical surface (8) will take the following form:

$$\begin{cases} X = \rho cos(\varphi), \\ Y = \rho sin(\varphi), \\ Z = F(\rho) + p\varphi, \end{cases} \tag{9}$$

where

$$F(\rho) = F_1(\rho) - p\tau.$$

Here (ρ, φ) are the curvilinear coordinates of a point on a helical surface; if φ = *const*, then we have the generating L, and if ρ = *const*, then we have a helical line. The function *F(ρ)* determines the law of change of the Z-coordinate of the current point of the guide L, and it can be written as follows:

$$F(\rho) = F(\tau) - p\tau = z - p\tau. \tag{10}$$

The geometric content of the function (10) is easy to find if we substitute φ = 0 into the system of Equation (9). Then, we will obtain the following equation system in parametric form:

$$\begin{cases} X = \rho, \\ Y = 0, \\ Z = F(\rho), \end{cases}$$

or, after removing the parameter ρ,

$$\begin{cases} Y = 0, \\ Z = F(x). \end{cases} \tag{11}$$

The system of Equation (11) determines the line of intersection of the helical surface with the *X0Z* plane; i.e., it analytically describes the axial section of the convolute helical surface.

2.3.2. The Influence of the Back-Rake Angle at the Nose of the Lathe Tool on the Profile of the Helical Convoluted Surface

From the triangle OM_1M_2 (Figure 5), we can determine the value of the radius of the main cylinder r_1:

$$r_1 = r_a cos(\theta) = r_a cos\left(\frac{\pi}{2} - \gamma\right) = r_a sin\gamma. \quad (12)$$

Since the axis OX is taken as the polar axis, the polar coordinates (ρ,τ) will determine the position of the segment AM_2, which is the projection of the cutting edge AD on the $X0Y$ plane.

Let the point M_2 be one of the arbitrary points of the segment AM_2; then, the curvilinear coordinate ρ will be the segment of variable value $|OM_2|$. Using the triangle OM_1M_2 and using Formula (12), we find the variable value ρ:

$$\rho(\tau) = \frac{r_a sin\gamma}{cos\left(\tau + \frac{\pi}{2} - \gamma\right)} = \frac{r_a sin\gamma}{sin(\gamma - \tau)}. \quad (13)$$

The obtained Expression (13) corresponds to Formula (4), that is, the first of the equation system (3) of the cutting edge AD_i in cylindrical coordinates.

Using the theorem of sines, we find the value of the segment OAM_2 from the triangle (AM_2):

$$|AM_2| = \frac{r_a sin\tau}{sin(\gamma - \tau)}.$$

From the right-angled triangle AD_iM_2, we can obtain the value of the segment length (D_iM_2):

$$|D_iM_2| = tan(\alpha_1)|AM_2| = tan(\alpha_1)\frac{r_a sin\tau}{sin(\gamma - \tau)}.$$

Since the point M_2 is accepted by us as arbitrary, it can be assumed that the length of the segment D_iM_2 is a variable value and corresponds to the 3-coordinate of an arbitrary point of the cutting edge AD_i in cylindrical coordinates. So instead of $|D_iM_2|$, we substitute $Z(\tau)$:

$$Z(\tau) = tan(\alpha_1)\frac{r_a sin\tau}{sin(\gamma - \tau)}. \quad (14)$$

The obtained Equation (14) corresponds to the system of Equation (3), which describes the generatrix L in cylindrical coordinates.

According to Formula (6) and using Formula (13), we solve that equation with respect to τ:

$$\tau = \gamma - arcsin\left(\frac{r_a sin\gamma}{\rho}\right). \quad (15)$$

The next step according to Formula (7) should be the solution of the Z-coordinate with respect to ρ; that is, Formula (15) should be substituted into Equation (14). Therefore, we obtain the following dependence:

$$z(\rho) = tan(\alpha_1)\frac{r_a sin\left(\gamma - arcsin\left(\frac{r_a sin\gamma}{\rho}\right)\right)}{sin\left(\gamma - \left(\gamma - arcsin\left(\frac{r_a sin\gamma}{\rho}\right)\right)\right)}.$$

After some reductions, the resulting equation will take the following form:

$$z(\rho) = tan(\alpha_1)\rho\frac{sin\left(\gamma - arcsin\left(\frac{r_a sin\gamma}{\rho}\right)\right)}{sin\gamma}. \quad (16)$$

To obtain the system of equations of the helical surface according to Formula (9), function (16) should be transformed according to Formula (10), and as a result, according

to Formula (11), the equation of the axial section of the convoluted helical surface should be obtained [76]:

$$Z(x) = tan(\alpha_1)x\frac{sin\tau}{sin\gamma} - \frac{P}{2\pi}\tau, \quad (17)$$

where the following definitions hold:

τ is one of the curvilinear coordinates of the cutting edge, determined by the formula

$$\tau = \gamma - arcsin\left(\frac{r_a sin\gamma}{x}\right);$$

P is the pitch of the specified thread;

γ is the rake angle;

α_1 is the half-profile angle of the cutting edge in the rake plane.

The received transcendental Equation (17) of the axial profile of the convolute helical cut made by the cutter indicates its theoretical discrepancy with the profile of the Archimedean thread given by the standard, which is described by the algebraic equation of the first order (1).

However, $\tau = 0$, $\frac{sin\tau}{sin\gamma} = 1$, and $\frac{P}{2\pi}\tau = 0$; if the angle γ approaches 0, then Equation (17) becomes equivalent to Equation (1).

The authors of the study [71], due to the algorithm developed by the authors, concluded that it is admissible to use threaded cutters with a back-rake angle of $\gamma = 12^\circ$ for the manufacture of a tool-joint thread 2 7/8 Reg. At the same time, the deviation from the nominal half-profile angle is less than 0.1°, which is less than 15% of the tolerance. In the article [68], the authors proposed a scheme for ensuring a negative rake angle due to a simple geometric change of the holder of a conventional thread cutter (Figure 6). With such a change, there is no need to create a new cutting insert or a method of its attachment at a certain back-rake angle γ.

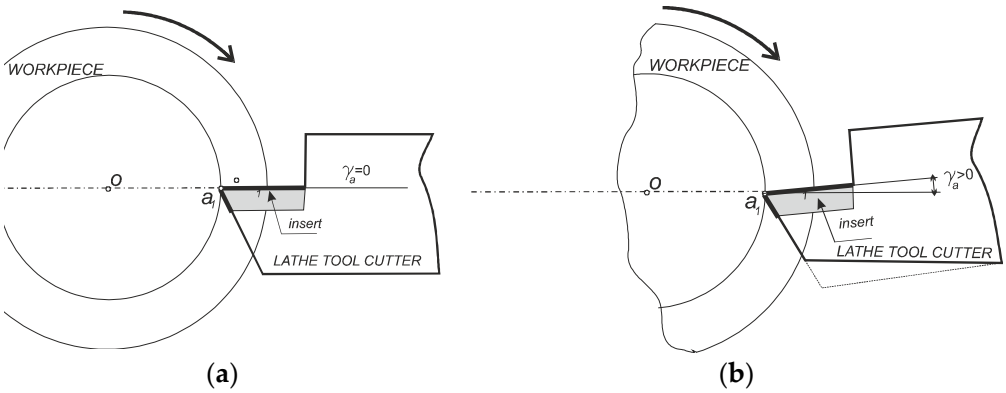

Figure 6. The scheme of ensuring the specified value of the back-rake angle γ: (**a**) conventional tool with back-rake angle $\gamma = 0$; (**b**) modernized tool shank with a changed tool base with back-rake angle $\gamma < 0$.

2.4. Analytical Method of Screw Thread Model Using Tool Cutting-Edge Inclination Angle Parameter

In fact, the surface of the convoluted helicoid is also obtained due to the inclination of the cutting insert at an angle λ relative to the axis of the thread, which is recommended to improve the operating conditions of the cutter (Figure 7). The angle λ is chosen so that it corresponds to the range between the angle of inclination of the screw on the depressions ψ_{BH} and on the protrusion ψ_3 ($\psi_{BH} < \lambda < \psi_3$).

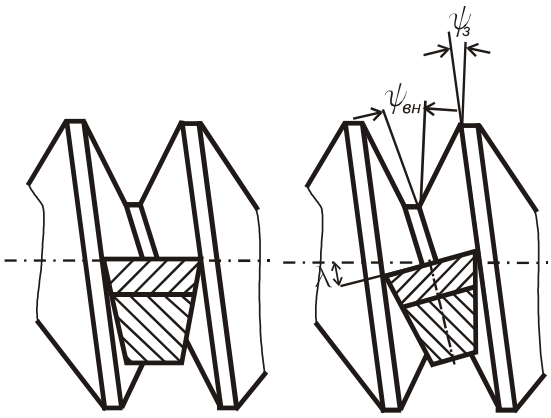

Figure 7. Scheme of installing the cutter perpendicular to the inclination of the screw turn: on the **left**—without the inclination of the cutting insert ($\lambda = 0$); on the **right**—with the inclination of the cutting insert ($\lambda > 0$).

Such an angle for tool joints is quite insignificant; it does not cause alarm among manufacturers regarding the influence on the accuracy of the thread profile, and therefore, the operating instructions for threaded cutters contain the method of using tools containing a plate installed at an angle relative to the axis of the thread. However, for large-pitch screw surfaces, including conical ones, the influence of the angle of inclination of the tool on the accuracy of their axial cross-section, that is, the thread profile, turns out to be quite significant [22,78]. It has been proven that for high-precision worm drives, reducing backlash with a high degree is quite a difficult task. This paper is based on the analysis of the accuracy of the kinematics of manufacturing convolute and involute worm screws, but it does not focus on the geometric parameters of the tools for their manufacture. In the study [79], the authors Onysko and Kopei used application shown in [80] to prove by calculations that the presence of a screw lead angle of $\lambda = 2.24^\circ$ for the NC10 tool-joint thread (the smallest size drill-string connect thread), and accordingly, the angle of inclination of the cutting edge of the cutter $\lambda_z = 2.24^\circ$, causes a decrease in the half-profile angle $\alpha/2$ by 0.24°, which is more than 30% of the tolerance. Description of the visual algorithm is presented on the pages 350–360 of work [80]. The methodology of the theoretical part of that research is essentially a continuation of the approaches presented in Figure 5 and described by Equation (17).

In Figure 8, a scheme is presented for compiling an algorithm for calculating the deviation of the received profile of the convolute surface from the profile of the thread specified by the standard, depending on the angle of inclination of the cutting edge of the thread cutter λ_z. The scheme is built in cylindrical coordinates. The Z-axis of the coordinate system coincides with the axis of the screw. The value r_1 denotes the radius of the main cylinder on which the guide helix of the convolute screw is placed, and r_a and r_d correspond to the scheme of the conical cut in Figure 2. The $X0Y$ plane is perpendicular to the Z-axis and contains the point of origin of coordinates O [80].

The generator AD_i of the convolute screw crosses the X-axis at point A, and it is inclined to the $X0Y$ plane at an angle σ. The projection of the generatrix AD_i on the $X0Y$ coordinate plane is the straight line AM_2, which forms an angle η with the X-axis. The segment AD_i belongs to the creation and is the left cutting edge of the cutter. The right cutting edge AB_i together with the left AD_i form a flat rake surface of the B_iAD_i cutter, which is highlighted in grey. The B_iAD_i plane is inclined to the XZ plane at an angle λ [80].

In polar coordinates, which are part of the cylindrical system, the line AM can be defined by the rotation angle τ of an arbitrary point M_2, lying on this line around the origin of the coordinate system O, as well as the length of the radius vector OM_2.

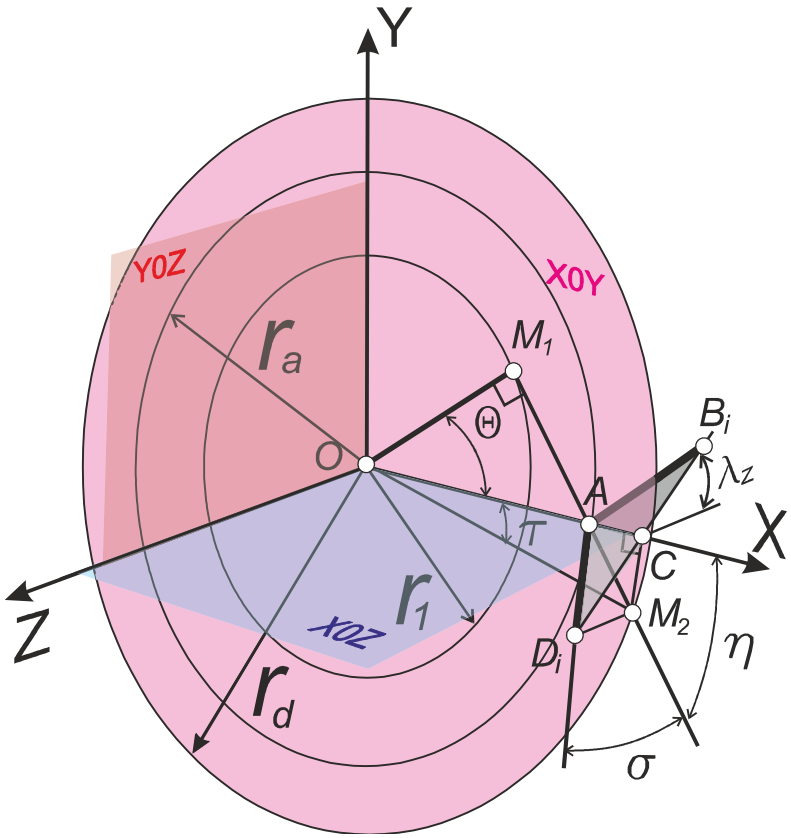

Figure 8. Scheme for calculating the deviation of the received profile of the convolute surface from the given profile of the thread.

In the *X0Z* plane, similarly to Formula (17), we obtain the analytical expression of the axial section of the convoluted helical surface:

$$Z(x) = tan(\sigma)x\frac{sin\tau}{sin\eta} - \frac{P}{2\pi}\tau, \tag{18}$$

where the following definitions hold:

τ is one of the curvilinear coordinates of the cutting edge, determined by the formula

$$\tau = \eta - arcsin\left(\frac{r_a sin\eta}{x}\right); \tag{19}$$

P is the pitch of the specified thread.

Since the input data are the angle of inclination of the cutting edge λz and the height of the fundamental triangle of the cut H, the functional dependence of the values η and σ on them should be detected.

According to Figure 1,

$$|DC| = \frac{P}{2}, |AC| = H - \frac{Ptan(\varphi)}{2} = \frac{2H - Ptan(\varphi)}{2}.$$

Since the cutter has a full profile,

$$|D_iC| = |DC| = \frac{P}{2},$$

From the triangle CD_iM_2 (Figure 8), we have $|CM_2| = \frac{Psin\lambda_z}{2}$.

From the triangle ACM_2, we have $tan(\eta) = \frac{|CM_2|}{|AC|}$. So,

$$\eta = arctan\left[\frac{Psin\lambda_z}{2\frac{2H-Ptan(\varphi)}{2}}\right] = arctan\left(\frac{Psin\lambda_z}{2H - Ptan(\varphi)}\right). \quad (20)$$

From the triangle D_iAM_2, we obtain the following ratios:

$$tan(\sigma) = \frac{|D_iM_2|}{|AM_2|}.$$

At the same time,

$$|D_iM_2| = |D_iC|cos\lambda_z,$$
$$|AM_2| = \frac{|AC|}{cos\eta} = \frac{2H-Psin(\varphi)}{2cos\eta}.$$

So,

$$tan(\sigma) = \frac{Pcos\lambda_z cos\eta}{2H - Ptan(\varphi)} = \frac{Pcos\lambda_z}{2H - Ptan(\varphi)} cos\left(arctan\left(\frac{Psin\lambda_z}{2H - Ptan(\varphi)}\right)\right). \quad (21)$$

Analytical dependences (18)–(21) obtained in this way describe the axial section of the convolute helical surface, which is obtained by a cutter with a non-zero angle of inclination of the cutting edge.

The obtained dependences (18)–(21) under the condition of zero value of the angle λ_z describe the profile of the Archimedean screw according to Equation (1).

However, $\tau = 0$, $\frac{sin\tau}{sin\gamma} = 1$, and $\frac{P}{2\pi}\tau = 0$, $tan(\sigma) = \frac{P}{2H} = \alpha$; if λ_z approaches 0, then Equation (18) becomes equivalent to Equation (1).

The study [81] proves the functional influence of the angle of inclination of the grinding tool on the profile of the resulting screw and proposes an algorithm for obtaining the axial profile of a polished worm screw. The angle of inclination of the grinding profile tool is one of the parameters of the methodology and application support presented in the study [82] for the accurate processing of conical worm screws with various curved axial profiles.

The profiling of tools for the process of whirling turning of worm shafts *ZA* (Archimedean profile) and *ZI* (involute profile) is presented in the study [78]. This paper does not contain analytical studies on convoluted helical surfaces. Considering the functional dependencies of worm surface profiles on cutting-edge profiles of tools for their production, the rake angle always has zero value only.

Therefore, the combined influence of the angle of inclination of the cutting edge and the rake angle of the tool on the value and accuracy of the half-profile angle based on the convolute approach to the formation of a conical large-pitch thread is an unsolved problem. Therefore, the goal of this study is to build an analytical model of profiling a triangular conical section using cylindrical coordinates and its verification based on the created algorithm and thread profile computer modeling. Attention should be paid to the fact that the cylindrical coordinates most accurately correspond to the model of the formation of helical surfaces since they fully correspond to the movements of forming: the translational movement of the cutting edges along the *Z*-axis of the thread and at the same time their rotational movement around it.

3. Theoretical Results

3.1. Function Dependence of Thread Profile on Double Parameter: Rake and Cutting-Edge Inclination Angle

Since the drill-string thread is tapered, the fundamental triangle thread *BAD* (Figure 1) has sides with different lengths.

The length of the long side *AB* is as follows:

$$|AB| = \frac{H \cdot cos\varphi}{sin(2\alpha - \varphi)}. \quad (22)$$

The length of the short side AD is as follows:

$$|AD| = \frac{H \cdot cos\varphi}{sin(2\alpha + \varphi)}, \tag{23}$$

where φ is the taper angle of the thread.

These formulas are necessary to establish the desired algorithm in relation to the drill-string tapered thread.

Therefore, the calculation scheme for placing the plane of the rake surface of the AB_iD_i of the lathe cutting tool (light pink) is built in the cylindrical coordinate system and the Cartesian coordinate system XYZ combined with it, with the coordinate planes $X0Z$ (purple), $Y0Z$ (lime), and $X0Y$ (pink) (Figure 9).

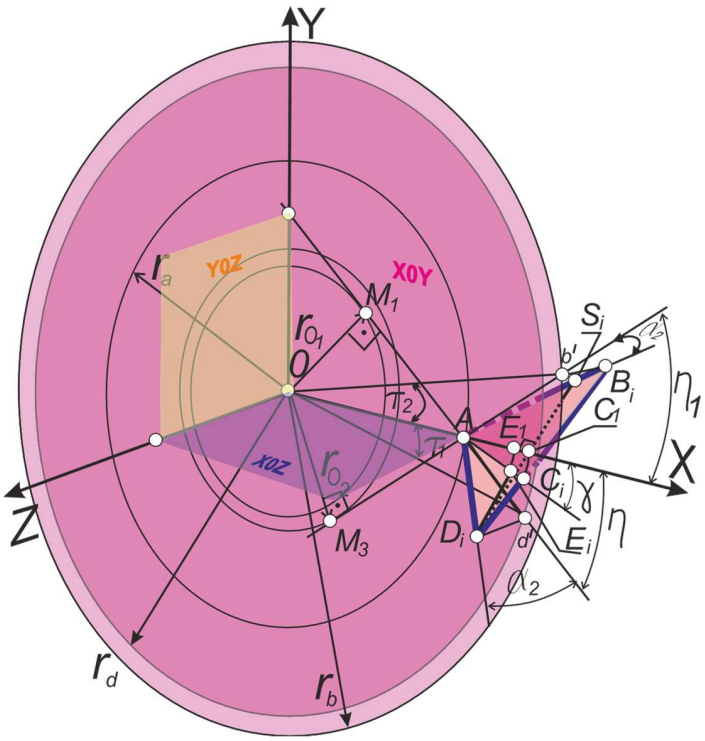

Figure 9. Scheme of placing the rake plane of the AB_iD_i cutting tool in the cylindrical coordinate system.

Mutually perpendicular segments (D_iS_i) and (AC_i) are placed on the front plane. The segments intersect at point E_i. Points A, E_i, and C_i lie in the coordinate plane $X0Y$ (pink). The angle between the axis X and the straight line AC_i is the rake angle γ at point A. The segment Ad' is the projection of the segment AD_i on the XOY plane. The segment Ab' is the projection of the segment AB_i on the plane XOY. Each of the specified projections is inclined to the X-axis at angles η and η_1, respectively. The length of the segment D_id' is the applicate (coordinate on the Z-axis) of the point D_i. The length of the segment D_ib' is the applicate (coordinate on the Z-axis) of the point B_i.

The segment AD_i is the left-hand cutting edge of the cutter, and therefore, it is the generator of the helicoid. It is placed at an angle α_2 to the $X0Y$ plane. Segment AB_i is the right-hand cutting edge of the cutter, and therefore, it is also the generating edge of the screw. It is also placed at an angle α_2 to the $X0Y$ plane. For ordinary cutters, the values of these angles are equal to the standard half-profile angle $\alpha = 30^\circ$. Point M_1 is the point of contact of line $d'M_1$ to the main cylinder with radius r_{o1}. Point M_2 is the point of contact of the line $b'M_2$ to the main cylinder with radius r_{o2}. The angle τ is the polar angle of an arbitrary point of the segment Ad', and the angle τ_1 is the polar angle of an arbitrary point of the segment Ab' (Figures 9 and 10).

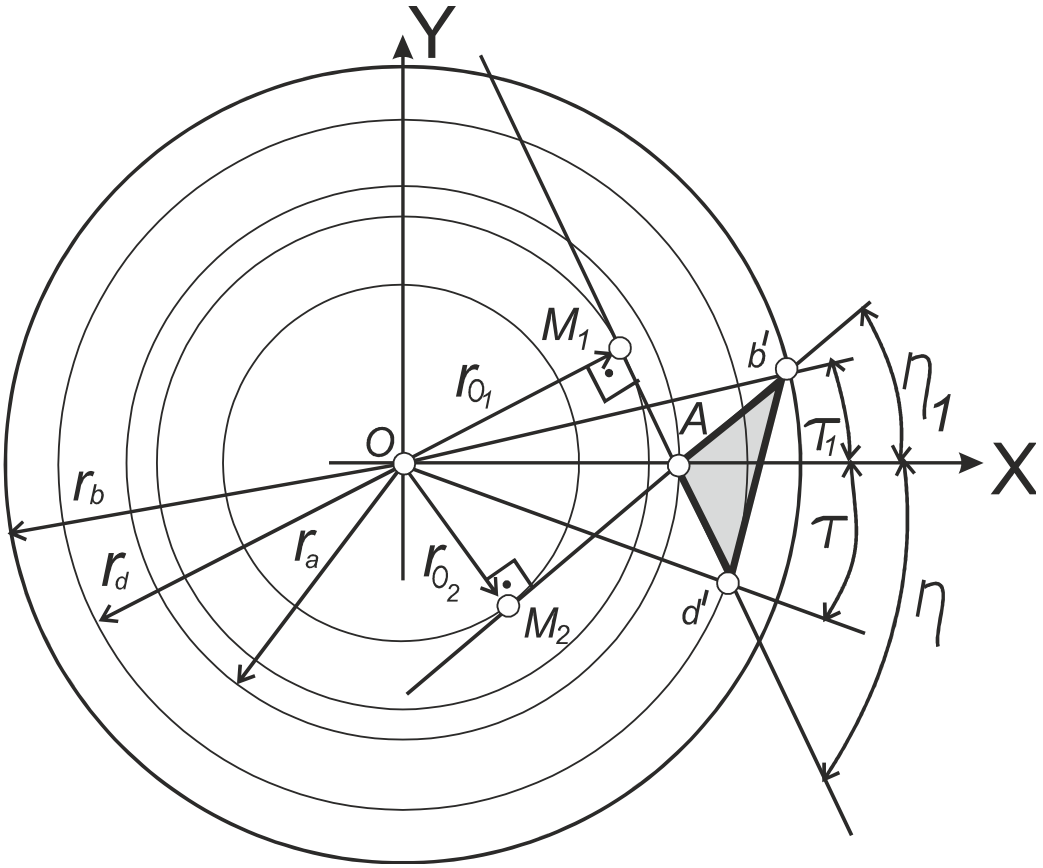

Figure 10. Diagram of placement of the rake plane projection of the lathe tool $A\ b'd'$ in the polar coordinate system.

Thus, by analogy with Formula (14), the Z-coordinates of the points of the generating AD_i depending on the angle of rotation τ, the X-coordinates, and the value of the radius r_a can be found by the equation

$$Z(x) = tan(\alpha)x\frac{sin\tau}{sin\eta} - \frac{P}{2\pi}\tau, \tag{24}$$

where

$$\tau = \eta - arcsin\left(\frac{r_a sin\eta}{x}\right). \tag{25}$$

So, by analogy with Formula (14), the Z-coordinates of the points of the generating AB_i depending on the angle of rotation τ_1, the X-coordinates, and the value of the radius r_b can be found by the equation

$$Z(x) = tan(\alpha)x\frac{sin\tau_1}{sin\eta_1} - \frac{P}{2\pi}\tau_1, \tag{26}$$

where

$$\tau_1 = \eta_1 - arcsin\left(\frac{r_a sin\eta_1}{x}\right). \tag{27}$$

For the completeness of Expressions (24)–(27), it is necessary to establish the algorithms for finding angles η and η_1.

3.2. Definition of Angles η and η_1

Figure 11 shows a complex drawing of the plane ABD of the rake surface of the thread cutting tool of the general position. The projection plane π_1 corresponds to the reference

plane at the nose point A. Through point A, the X-axis is drawn, which corresponds to the X-axis illustrated in Figures 9 and 10. The axes Y and Z also correspond to the axes of the same names in Figure 9. The XOY plane is parallel to the frontal plane of the π_2 projections. The plane XOZ coincides with the main reference plane at point A; i.e., it is parallel to the horizontal plane of projections π_1. The YOZ plane is parallel to the π_3 projection plane.

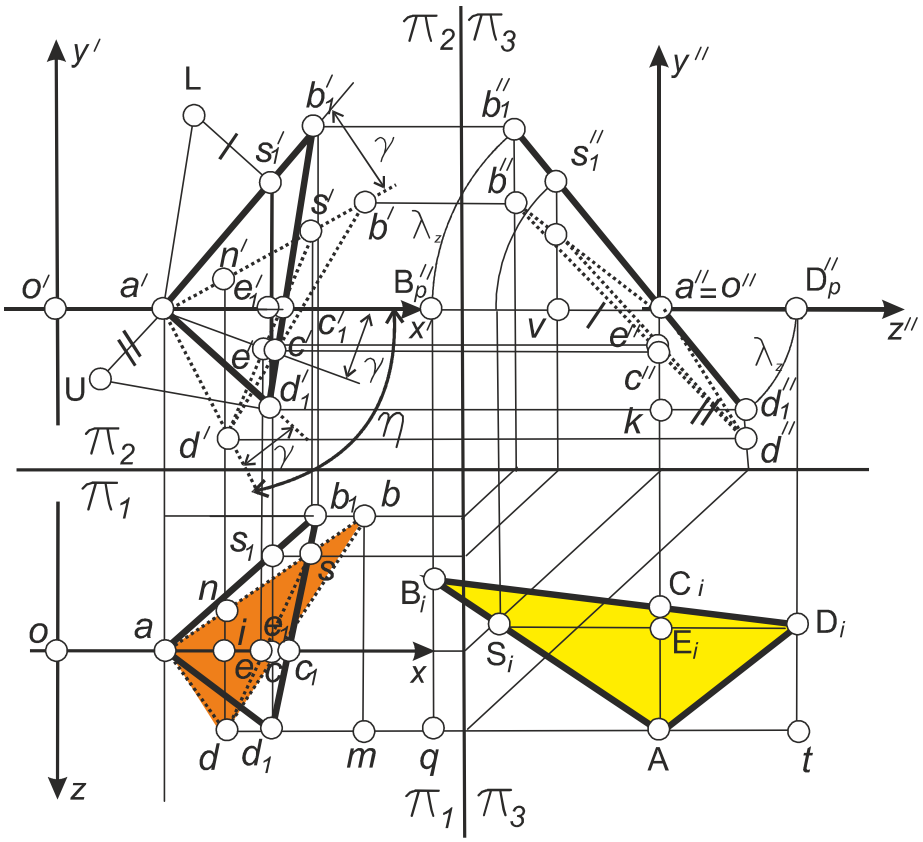

Figure 11. Complex drawing of the plane of the rake surface ABD of the lathe tool, which is placed under the angle of inclination λ_z and the rake angle at the nose point γ.

The rake plane of the cutting tool AB_1D_1 is constructed as a plane that is perpendicular to the plane of projections π_3. This plane is marked with bold lines. Its projection onto the π_3 plane is denoted by $b_1''a''d_1''$. The natural value of the angle λ_z is placed on the projection plane π_3. This angle corresponds to the angle of rotation of the specified plane around the X-axis. Considering the fact that the Z-axis in the cylindrical coordinate system is constructed as the axis of the screw thread, it means that the angle λ_z is the angle of setting the plane AB_1D_1 relative to the plane of the axial section of the screw.

Within the AB_1D_1 plane, the segment AC_1 is constructed; it lies on the X-axis, and the segment D_1S_1 is perpendicular to it. The segments intersect at point E_1.

The rotation of the plane AB_1D_1 by an angle γ is carried out in the plane XOY, which coincides with the reference plane at point A. Thus, all points of the plane AB_1D_1 are rotated by an angle γ around an axis that is parallel to the Z-axis and passes through point A. Therefore, on the π_2 projection plane, the angle γ is reflected in its natural form. As a result of the rotation, the plane ABD was formed (it is highlighted with dashed lines). The specified plane is the desired plane of the rake surface of the thread cutting tool, and its horizontal projection abd (orange) corresponds to the given fundamental triangle of the tapered thread ABD from Figures 1 and 2.

The natural appearance of the triangle of the cutting edge of the cutter, which is intended to form the fundamental triangle ABD, is shown in Figure 11 in the form of a triangle AB_iD_i (yellow). The specified triangle is constructed by combining the projection

of $a''b_1''d_1''$ with the plane XOZ, i.e., by turning the plane AB_iD_i around the X-axis by an angle λ_z, which is naturally equal to the lead angle of the helix ψ.

The angle η is the angle of inclination of the frontal projection of the cutting edge AD_i to the XOZ plane (Figure 9), which means $a'd_1'$ to the $x's$ axis (Figures 10 and 11). It can be defined as the sum of the angle γ and the angle $d_1'a'e_1'$. So, we will determine the indicated angle according to the equation

$$\eta = \gamma + \angle d_1'a'e_1'. \tag{28}$$

From the right triangle $d_1'a'e_1'$, the angle $d_1'a'e_1'$ can be determined using the following formula:

$$\angle d_1'a'e_1' = arctan\left[\frac{|d_1'e_1'|}{|a'e_1'|}\right], \tag{29}$$

where $|d_1'e_1'|$ equals $|a'k'|$ (Figure 11), which can be determined from the right triangle $d_1''ka''$ as follows:

$$|d_1'e_1'| = |a''k| = tg(\lambda_z)|kd_1''| = tg(\lambda_z)|di|, \tag{30}$$

where $|di|$ is determined from the right triangle dai (Figure 11):

$$|di| = sin(\angle dai) \cdot |ad| = sin(\alpha)|AD|. \tag{31}$$

So, after Equation (31) is inserted into it, Formula (30) will look like

$$|d_1'e_1'| = tan(\lambda_z)sin(\alpha)|AD|. \tag{32}$$

$|a'e_1'|$ is defined from right triangle $d_1'a'e_1'$ due to the expression (Figure 11)

$$|a_1'e_1'| = \sqrt{|a_1'd_1'|^2 - |d_1'e_1'|^2}, \tag{33}$$

where the following definitions hold:

$|d_1'e_1'|$ is defined by the Equation (30);

$|a'd'_1|$ can be determined using a right triangle $ua'd'_1$, in which the segment (ua') is set at right angles to the segment $a'd'_1$ and is equal in size to the length of the segment kd''_1, i.e., the difference in the coordinates of the points k and d''_1 in the plane of projections π_3.

Based on the method of finding the actual values of the segment lengths in the sketch geometry, the constructed right triangle contains the segment ud'_1, which is the real value of the segment AD_i, i.e., the real value of one of the two lateral cutting edges of the cutter. Since in Figure 11, the real appearance of the triangle of the cutting edge of the cutter is displayed as AB_iD_i, we have the following expression:

$$|ud_1'| = |AD_i|.$$

Thus, the length of the segment $a'd'_1$ from the triangle $ua'd'_1$ will be determined by the following equation:

$$|a'd_1'| = \sqrt{|ud_1'|^2 - |ua'|}^2 = \sqrt{|AD_i|^2 - |kd_1''|^2}, \tag{34}$$

where

$$|kd_1''| = |a''d_1''| \cdot cos\lambda_z,$$

where

$$|a''d_1''| = |E_iD_i| = |AD_i| \cdot sin(\angle E_iAD_i).$$

So, taking into account that the profile of the cutting edge and thread profile are the same, i.e., $|AD_i| = |AD|$, we obtain the following expression:

$$|a'd_1'| = |AD|\sqrt{1 - sin^2\alpha cos^2\lambda_z}. \tag{35}$$

Thus, Formula (33) will take the following form:

$$|a_1'e_1'| = \sqrt{\left(|AD|\sqrt{1 - sin^2\alpha cos^2\lambda_z}\right)^2 - (tan\,(\lambda_z)sin(\alpha)|AD|)^2}.$$

And after certain manipulations, this equation received the following definition:

$$|a_1'e_1'| = |AD|\sqrt{1 - sin^2\alpha(cos^2\lambda_z - tan(\lambda_z)^2)}. \quad (36)$$

According to Formulas (28) and (29) and considering Expressions (32), (33), and (37), η is defined as follows:

$$\eta = \gamma + arctan\left(\frac{tan(\lambda_z)sin(\alpha)}{\sqrt{1 - sin^2\alpha(cos^2\lambda_z - tan(\lambda_z)^2)}}\right). \quad (37)$$

Using Figure 11 in a similar way, the formula for determining the angle η_1 can be derived:

$$\eta_1 = arcsin\left(\frac{sin\alpha sin\lambda_z}{\sqrt{1 - sin^2\alpha cos^2\lambda_z}}\right) - \gamma. \quad (38)$$

So, the group of Equations (24)–(27), (37), and (38) is the analytical model of the side profile of a tapered thread with a given triangular or trapezoidal profile, which is a function of the thread diameter and pitch, as well as the geometric parameters of the cutting tool: the rake angle, the angle of inclination, and the half-profile angle of its cutting edge.

According to Formulas (37) and (38), the angle $\eta = \eta_1 = 0$, if $\gamma = \lambda_z = 0$, and therefore, according to Formulas (24) and (25), $Z(x) = tan(\alpha)x$, which corresponds to Formula (1).

4. Modeling a Tapered Thread Profile for Drill Strings

On the basis of the algorithm (24)–(27), (37), and (38), a visual application program was developed for obtaining the calculated drill-string tool-joint thread profile, the standard sizes of which are regulated by the standard [63]. The standard regulates 31 standard sizes of tool-joint tapered threads, which are formed as external threads for the pin (Figure 12a) and as internal threads for the box (Figure 12b).

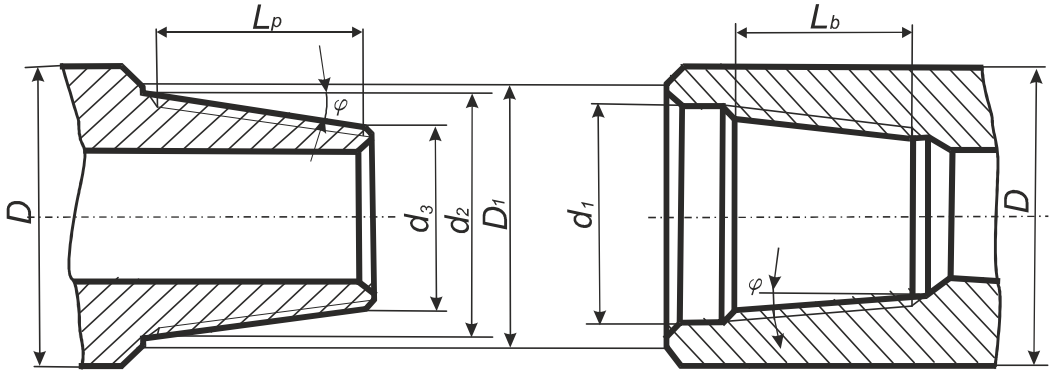

(**a**) (**b**)

Figure 12. Drawing of the drill-string tool-joint parts of the pin (**a**) and the box (**b**): φ is the taper angle, D is the outer diameter of the tool-joint tapered thread, D_1 is the diameter of the tool-joint tapered thread at the end section, d_1 is the diameter of the cylindrical twist, d_2 is the diameter of the larger base of the cone, d_3 is the diameter of the smaller base of the cone, L_p is the length of the threaded part of the pin, L_b is the length of the threaded parts of the box.

4.1. Investigation of NC23 Drill-String Tool-Joint Thread Profile Accuracy

The example concerns the standard size of the tool-joint thread NC23 based on the application of a special visual application program developed by the authors of this paper (Onysko and Kopei) based on the algorithm (24)–(27), (37), and (38). The visual application [80] is improved by using calculating the coordinates of the points of rectilinear sections of the thread profile (Figure 1). The input data for calculating the coordinates of the points of the thread fundamental triangle are the values of the parameters of a certain standard size and the values of the rake angle γ and the inclination angle of the cutting edge λ. This modeling example concerns one of the most common threaded profiles in the practice of using drill strings V-0.038R (Table 3). The profile is mostly recommended by standards GOST and API as having a reliability that is largely needed and therefore preferred in oil and gas extraction technology. This profile is used for the NC23 drill-string thread, which has the smallest diameter of the smaller base of the cone d_3 = 65 mm and at the same time the largest value of the step P, which means the largest value of the thread lead angle ψ, which is usually near or equal to the inclination angle of the cutting edge λ.

Table 3. Profile parameters of the drill-string tool-joint tapered thread NC23 according to the standard [63].

No.	Parameter Name, Dimension	Marking	Value
1	Pitch, mm	P	6.35
2	Tapered angle, °	φ	4.763
3	Thread height (not truncated), mm	H	5.487
4	Thread height (truncated), mm	h	3.095
5	Root truncation, mm	f_c	1.427
6	Crest truncation, mm	f_r	0.965
7	Angular depth, mm	h_1	2.633
8	The outer thread diameter of the small base of the cone of pin, mm	d_3	52.433
9	Half-profile angle, °	α	30

It is convenient to place the original point (0, 0) of the orthogonal coordinate system XZ for determining the profile of the thread on the axis of the thread and in relation to the root of the first turn at the point corresponding to the coordinate of point A on the Z-axis (Figure 13). Therefore, Z_a = 0. For the convenience of profiling and evaluation of the profiled longer and shorter flanks of the thread, two opposite-oriented axes are used: $-Z$ and $+Z$ (Figure 13). The points of the thread fundamental triangle are signed as in Figure 1: A, B, D, and an additional point C. The points of the thread profile that indicate its straight sections are marked by numbers: (3, 4) are points of the smaller flank; (5, 6) are points of the larger flank. The half-profile angles of the tool cutting edge are the same and have the designation α_1. For ordinary cutting tools, it is obvious that α_1 is equal to 30°. Half-profile angles of the obtained thread are signed differently: α_l is the half-profile angle formed by the larger flank of the thread profile; α_{sh} is the half-profile angle formed by the smaller flank of the thread profile.

With such a coordinate plan, the coordinates of the vertices of the fundamental triangle for each thread turn n can be determined by the following formulas:

$$X_a = nPtan(\varphi) + d_3/2 + f_c - H \text{ (mm)}, \tag{39}$$

$$X_d = nPtan(\varphi) + d_3/2 + f_c + tan(\varphi)F_r/2 \text{ (mm)}, \tag{40}$$

$$X_b = X_a + H + tan(\varphi)P/2 \text{ (mm)}. \tag{41}$$

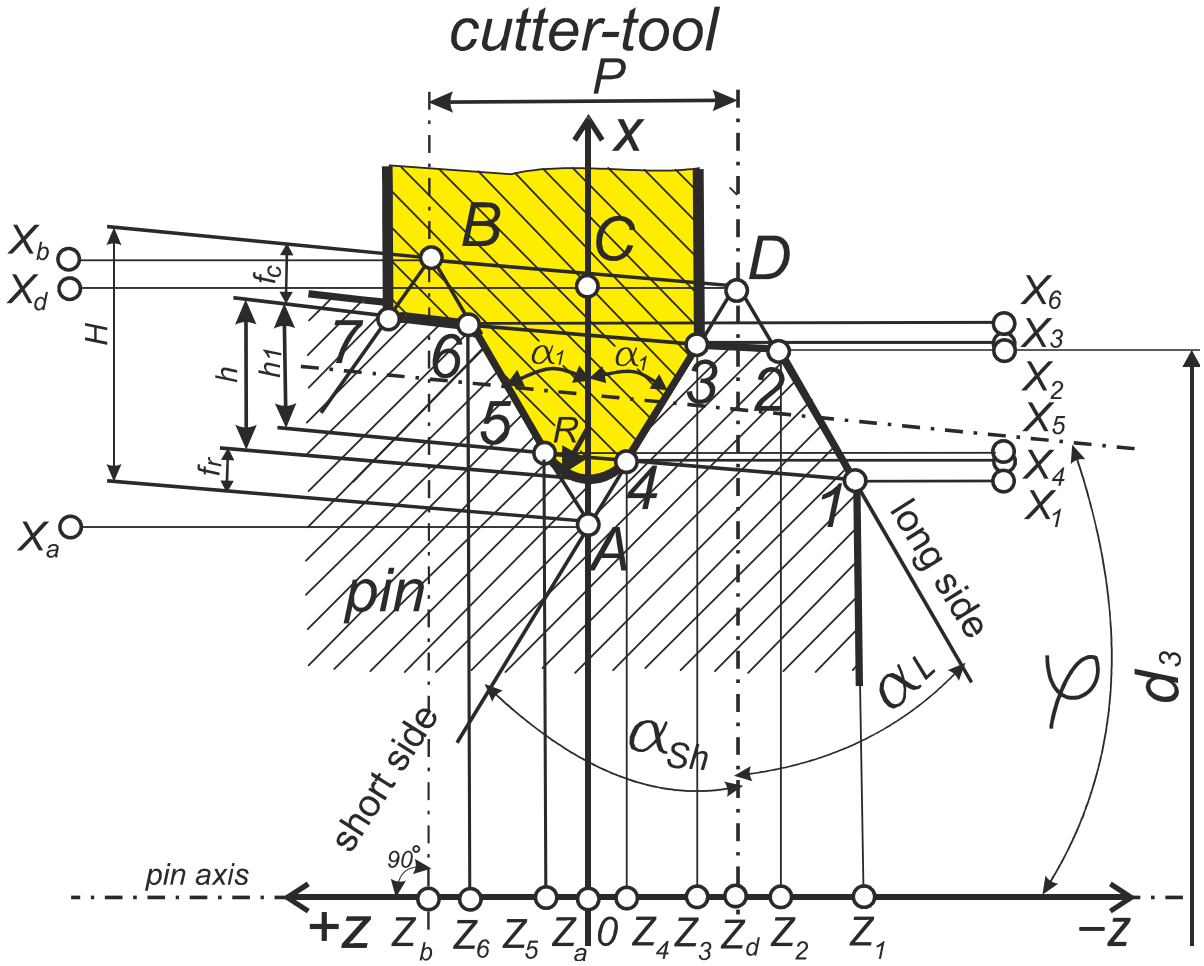

Figure 13. Scheme of obtaining the profile of a drill-string thread, which is made using the full-profile lathe thread cutting tool (yellow).

4.2. Visual Analytical Research of NC23 Made by Lathe Cutter with Zero-Angle Parameters

According to Equations (39)–(41), the *X*-coordinates of the vertices of the fundamental triangle *A*, *B*, and *D* are as follows (Figures 14 and 15):

$$X_a = 22.16 \text{ mm}, X_d = 27.65 \text{ mm}, X_b = 27.93 \text{ mm}.$$

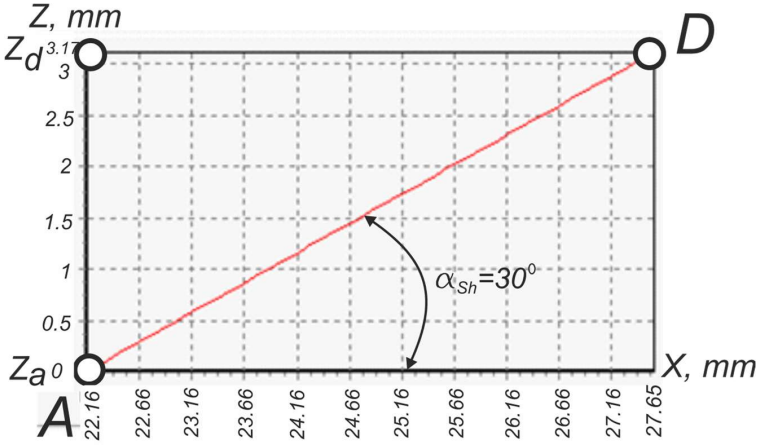

Figure 14. Visual software model of the flank profile *AD* of the drill-string tool-joint thread NC23.

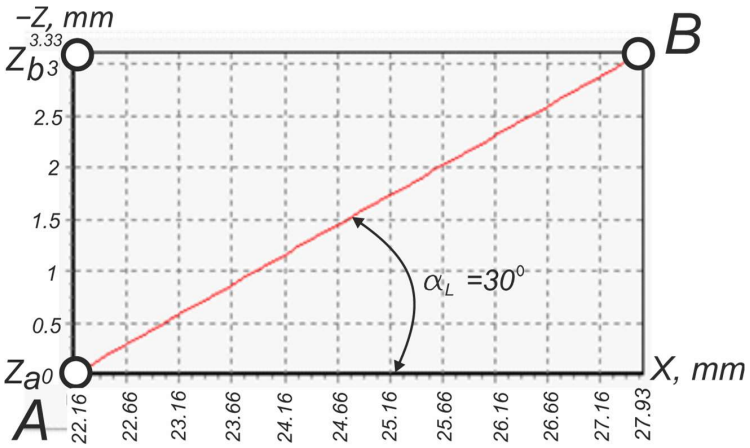

Figure 15. Visual software model of the flank profile *AB* of the drill-string tool-joint thread NC23.

Based on the algorithm (24)–(27), (37), and (38) and the data X_a, X_d, and X_b as well as the values $\gamma = 0$ and $\lambda_z = 0$, the values of the *Z*-coordinates of the vertices of the fundamental triangle *A*, *B*, and *D* were obtained: Z_d = 3.17 mm (Figure 14); Z_b = 3.33 mm (Figure 15).

Diagrams (Figures 14 and 15) obtained on the basis of visualization of the algorithm (24)–(27), (37), and (38) developed by Onysko and Kopei [80] show the rectilinear nature of the lateral fundamental profile of the NC23 thread under the condition of using a conventional threaded cutter with zero values of the rake angle $\gamma = 0°$ and the angle of inclination of the cutting edge $\lambda = 0°$.

The exact values of the coordinates Z_d = 3.17 mm and Z_b = 3.33 mm were obtained using the algorithm (24)–(27) and (38). Half-profile angles α_L and α_{sh} (Figures 14 and 15) are determined by the formulas

$$\alpha_L = arctan\left(\frac{z_b}{x_b - x_a}\right), \tag{42}$$

$$\alpha_{sh} = arctan\left(\frac{z_d}{x_d - x_a}\right). \tag{43}$$

After substituting the data X_a = 22.16 mm, X_d = 27.65 mm, X_b = 27.93 mm, Z_d = 3.17 mm, and Z_b = 3.33 mm in Formulas (42) and (43), we obtain

$$\alpha_L = \alpha_{Sh} = \alpha = 30°.$$

That is, both angles have the value prescribed by the standard. Therefore, according to Equation (1), the graphs in Figures 14 and 15 show the algebraic linear dependence

$$Z(x) = tan\left(\frac{\pi}{6}\right)x = 0.58x. \tag{44}$$

4.3. Visual Analytical Research of NC23 Made by Lathe Cutter with Non-Zero-Angle Parameters

All diagrams in the figures below were obtained using the application developed by Onysko and Kopei [80].

The inclination angle of the cutting edge, λ_z, is defined as equal to the lead angle of the screw on the outer diameter at a given turn of the thread ψ_3 (Figure 7), which is determined by the formula

$$\psi_3 = arctan\frac{P}{\sqrt{(P{\cdot}tan(\varphi))^2 + \pi^2(d_3 + 2l{\cdot}tan(\varphi))^2}},$$

where *l* is the distance from the smaller base of the cone to a specific turn of the thread.

The value of the thread lead-angle ψ_3 can be determined at any distance *l* from the smaller base of the cone of the tapered thread to its larger base. If the distance *l* = 0, then

the lead angle of its maximum and its effect on the nature of the profile curve is obviously maximum. For the NC23 thread, it is $\psi_3 = 2.61°$. Therefore, it is accepted that the inclination angle of the cutting edge is equal to the following: $\lambda_z = \psi_3 = 2.61°$.

For reasons of graphical persuasiveness of the influence of the rake angle on the character of the side profile of the obtained thread, an excessively large value of the rake angle $\gamma = 50°$ was adopted (Figure 16).

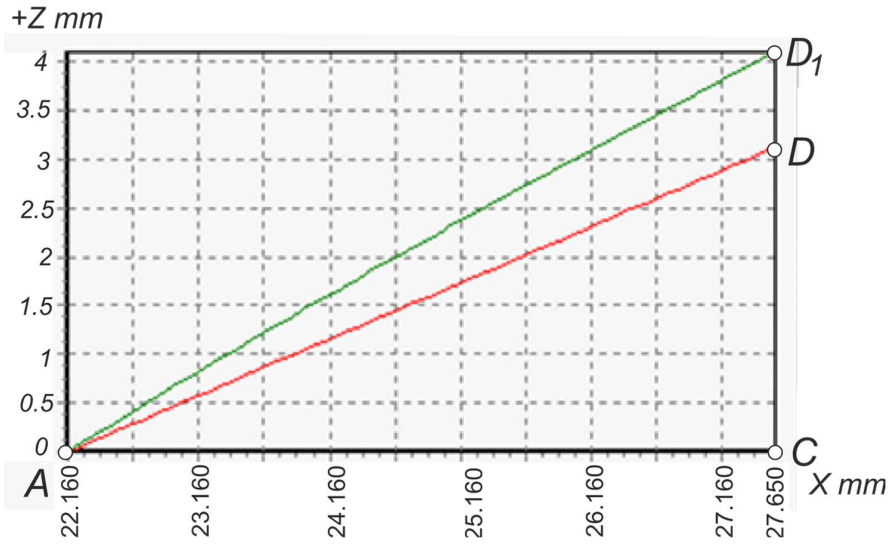

Figure 16. Comparison of models of the lateral theoretical profile of the NC23 thread: standard (red) and made by the tool with the geometric parameters of the cutter $\gamma = 50°$, $\lambda_z = 2.61°$ (green).

4.3.1. Analysis of the Flank Profile Models of Thread

The large visual difference between the standard profile and the predicted profile obtained under the condition of using the parameters $\gamma = 50°$ and $\lambda_z = 2.61$ proves the importance of analyzing the obtained data. The red line AD is the standard view of the side profile of the starting triangle of the conical keyhole. The inclination angle of the line AD relative to the X-axis is 30°, which corresponds to the standard value of the thread half-profile angle α_{sh} near its short side (Figure 17).

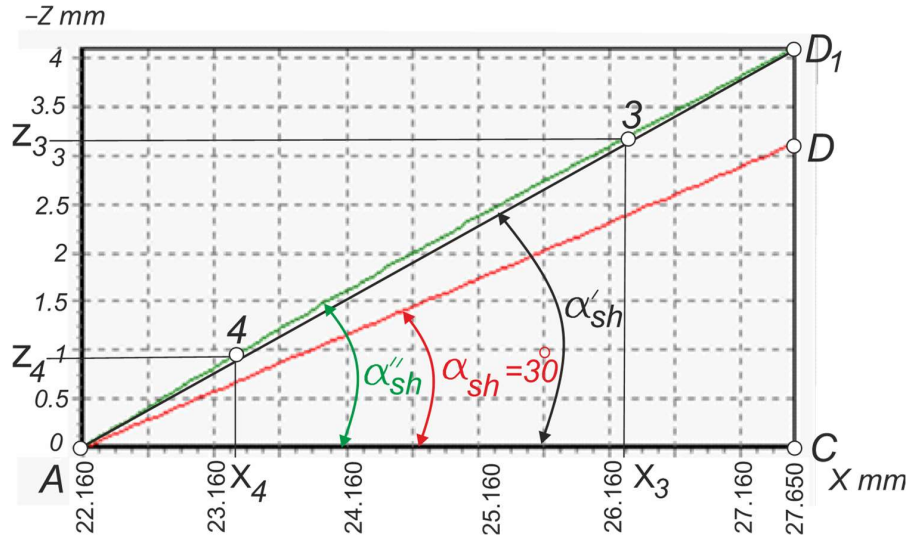

Figure 17. Comparison of models of the side profile of the NC23 thread: red straight AD—standard; green curve AD_1—predicted profile obtained using the tool with geometric parameters of the cutter $\gamma = 50°$, $\lambda_z = 2.61°$; black straight AD_1—linear interpolation of the green curve by two points.

The green line AD_1 is a curve obtained according to the algorithm (24)–(27), (37), and (38) of the profile of the fundamental triangle side according to the applied parameters of Table 1 and the geometric parameters of the cutting tool $\gamma = 50^\circ$ and $\lambda_z = 6.51^\circ$. The black line AD_1 is an interpolation of the two extreme points of the green curve. It is inclined to the X-axis at an angle α_{sh}, according to Formula (43), and therefore, the straight line AD_1 is described by the equation (Figure 15)

$$Z = \tan(\alpha_{sh'}) = \frac{|CD_1|}{|CA|} = \frac{(z_{d1-z_C})}{(X_C - x_A)}x. \quad (45)$$

By analogy, the line AB_1 is described by the equation

$$Z = \tan(\alpha_{l'}) = \frac{(z_{B1-z_C})}{(X_C - x_A)}x. \quad (46)$$

It is more correct to define the profile angle as the angle of inclination not of the lateral side AD, which refers to the original theoretical (fundamental) triangle, but of the lateral side between points 3 and 4 (Figure 13), which is actually part of the thread profile. On the diagram, Figure 17 is line (34), which is part of the green AD_1 curve. If we take it as a segment of the straight line (34) obtained by interpolation along the two extreme points 3 and 4, then the section of the profile of the thread (34) can be described by the equation

$$Z = \tan(\alpha_{sh''}) = \frac{(z_{3-z_4})}{(X_3 - x_4)}x, \quad (47)$$

where the angle $\alpha_{sh}{}''$ is the actual thread half-profile angle along its shorter side, obtained by a cutter with non-zero geometric parameters.

With such an orthogonal coordinate system, the coordinates of the vertices of the fundamental triangle for each turn of the thread n can be determined by the following formulas:

$$X_4 = X_d - f_c - h_1, \text{(mm)} \quad (48)$$

$$X_3 = X_d - f_c, \text{(mm)}, \quad (49)$$

where X_d is obtained from Formula (40).

Similarly, expressions can be obtained for determining the section of the actual thread between points 6 and 5 (Figure 13):

$$Z = \tan(\alpha_{l''}) = \frac{(z_{6-z_5})}{(X_6 - x_5)}x \quad (50)$$

where the angle $\alpha_l{}''$ is the predicted actual half-profile angle of the thread along its profile longer side, obtained by a cutter with non-zero geometric parameters.

$$X_5 = X_b - f_c - h_1, \text{(mm)} \quad (51)$$

$$X_6 = X_b - f_c, \text{(mm)}, \quad (52)$$

where X_b is obtained from Formula (41).

As a result of calculating the X-coordinates according to Formulas (48), (49), (51), and (52), as well as the corresponding Z-coordinates based on the algorithm (24)–(27) and (38), it is possible to give a predictive calculation of the half-profile angles of the NC23 thread obtained as a result of its production with a cutting tool with geometric parameters: rake angle $\gamma = 50^\circ$ and angle of inclination of the cutting edge $\lambda_z = 2.61^\circ$ (Table 4).

Table 4. Results of the predictive software calculation of half-profile angles of drill-string connecting thread NC23 α_{sh}', α_{sh}'', α_l', α_l'' obtained as a result of turning using a cutting tool with geometric parameters: rake angle $\gamma = 50°$ and inclination angle of the cutting edge $\lambda_z = 2.61°$.

Long Side	Root	Short Side	Short Side Truncated		Long Side Truncated	
			mm			
X_{b1}	X_a	X_{d1}	X_3	X_4	X_5	X_6
27.93	22.16	27.65	26.22	23.59	23.87	26.50
Z_{b1}	$Z_a = Z_c$	Z_{d1}	Z_3	Z_4	Z_5	Z_6
4.73	0	4.17	3.42	1.28	1.52	3.64
			Half-profile angles, °			
α_l'		α_{sh}'	α_{sh}''		α_l''	
39.34		37.22	39.14		38.87	

4.3.2. Modeling of the Side Profile of the NC23 Drill-String Thread Made by Turning Tool with Rake Angle $\gamma = 12°$

In the case of turning stainless steel threads, researchers often recommend a rake angle in the range of 8–12° [65,67]. The diagrams in Figures 18 and 19 show a certain visual difference between the actually straight standard profile and the side profile of the thread: *AB* in Figure 18 and *AD* in Figure 19. More precise numerical information obtained thanks to the predictive algorithm based on (24)–(27), (37), and (38) shows the possibility of using the rake angle $\gamma = 12°$ and the inclination angle of the cutting edge $\lambda_z = 2.61°$ as geometric parameters for turning threads from difficult-to-machine materials and at the same time ensuring the accuracy of the half-profile angle $\alpha = 30 \pm 0.75°$ (Table 5). The values of the predicted half-profile angles $\alpha_{sh}'' = 30.04°$ and $\alpha_l'' = 30.15°$ fall into this range and actually show that the excess of the angular size is less than 33% of the limit deviation tolerance. At the same time, it should be noted that the value of the angle $\alpha_l' = 30.58°$ indicates a deviation from the nominal, which reaches 73% of the tolerance. However, as can be seen from the diagram in Figure 17, the angles α_l' and α_{sh}' have exclusively research value and prove the non-linear nature of the predicted flank profile of the NC23 thread obtained using thread turning with the following geometric parameters: rake angle $\gamma = 12°$ and angle of inclination of the cutting edge $\lambda_z = 2.61$ °.

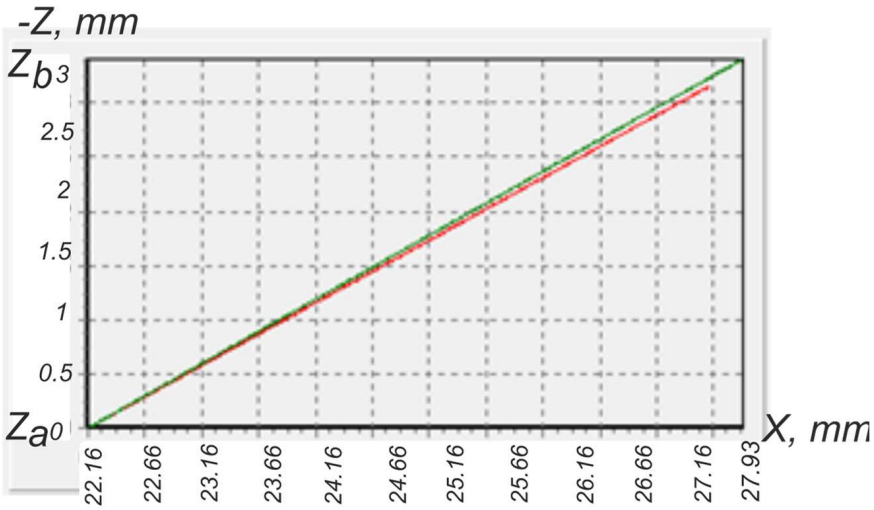

Figure 18. Comparison of the models of the side profile *AB* of the NC23 thread: standard (red) and made using the cutting tool with the geometric parameters of $\gamma = 12°$, $\lambda_z = 2.61°$ (green).

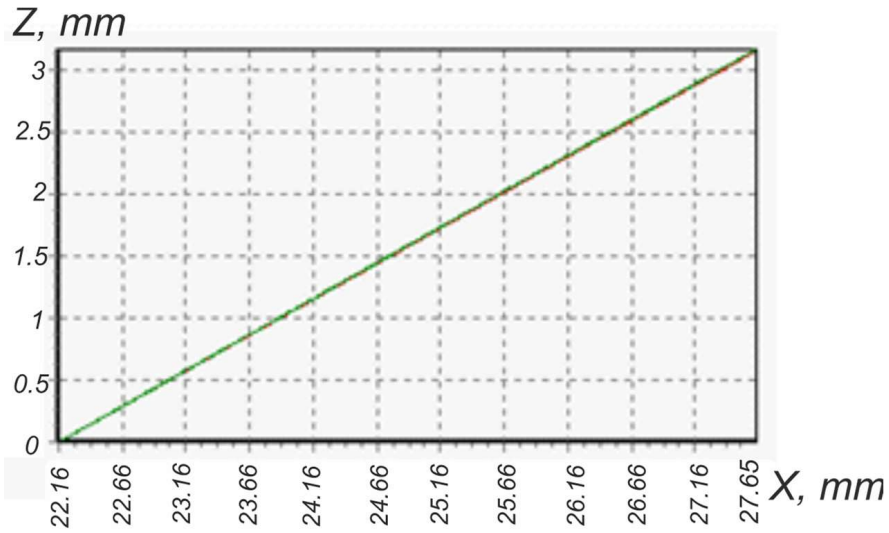

Figure 19. Comparison of the models of the side profile *AD* of the NC23 thread: standard (red) and made using the cutting tool with the geometric parameters of $\gamma = 12°$, $\lambda_z = 2.61°$ (green).

Table 5. Results of the predictive software calculation of half-profile angles of NC23 drill-string thread α_{sh}', α_{sh}'', α_l', α_l'' made using tools with the rake angle $\gamma = 12°$ and the inclination angle of the cutting edge $\lambda_z = 2.61°$.

Half-Profile Angles, °			
Side *AB*	**Side *AD***	**Flank 34**	**Flank 56**
α_l'	α_{sh}'	α_{sh}''	α_l''
30.58	30.08	30.04	30.15

4.4. The Results of Side Profile Modeling of the NC56 Drill-String Thread Made by Turning Tool with Non-Zero Rake Angle

For a complete illustration of the effect of the diameter of the part on the thread profile, let us use a drill-string thread of NC56 as an example, the diameter of which is greater than 117 mm (Table 6).

Table 6. Profile parameters of the drill-string tool-joint tapered thread NC56 according to the standard [63].

No.	**Parameter Name, Dimension**	**Marking**	**Value**
1	Pitch, mm	P	5.471
2	Tapered angle, °	φ	7°7′30″
3	Thread height (not truncated), mm	H	5.471
4	Thread height (truncated), mm	h	3.083
5	Root truncation, mm	f_c	1.423
6	Crest truncation, mm	f_r	0.965
7	Angular depth, mm	h_1	2.625
8	The outer thread diameter of the small base of the cone of pin, mm	d_3	117.5
9	Half-profile angle, °	α	30

The results of the predictive calculation of the half-profile angles α_{sh}', α_{sh}'', α_l', and α_l'' based on (24)–(27), (37), and (38) are presented in Table 7. This table refers to the application of rake angle values of $\gamma = 8°$, $\gamma = -8°$, and $\gamma = 4°$, which are often recommended in scientific sources. The results show that the half-profile angle along the short side is close in value for a negative and the same modulus of a positive rake angle. The half-profile angle, along the long sides, differs significantly when using positive or negative rake angles.

However, the deviation from the nominal value by 0.35° does not exceed 47% of the ±0.75° angle tolerance. At the rake angle $\gamma = 4°$, the nominal deviation is less than 0.1°, which is 13% of the tolerance (Table 7).

Table 7. Results of the predictive software calculation of half-profile angles of NC56 drill-string thread α_{sh}', α_{sh}'', α_l', α_l'' obtained as a result of turning using a cutting tool with the following geometric parameters: rake angle $\gamma = 8°$, $\gamma = -8°$, $\gamma = 4°$ and the inclination angle of the cutting edge $\lambda_z = 1.06°$.

Parameters		**Half-Profile Angles, °**			
		Side *AB*	**Side *AD***	**Flank 34**	**Flank 56**
λ, °	γ, °	α_l'	α_{sh}'	α_{sh}''	α_l''
1.060	−8	29.99	30.39	30.35	29.91
1.060	8	30.17	30.28	30.35	30.11
1.060	4	30.10	29.97	29.95	30.01

5. Conclusions

The triangular shape of the profile specified by the standard cannot be obtained for the surface of cylindrical and conical screw threaded parts, which are made with the help of turning cutters of high productivity. For the production of threaded parts from materials with different machinability characteristics, including difficult-to-machine steels, there is a need to use specially oriented cutting edges relative to the axis of the parts. The consequences of this are as follows:

- For an effective threading process on workpieces made of different machinability materials, cutters should be used with selected non-zero geometric parameters, namely the rake angle and the inclination angle of the cutting edge. This causes the surfaces of the conical or cylindrical threads to be obtained with the help of the specified cutters which consist of two convolute helicoids.
- The axial profile of a thread formed in this way does not contain rectilinear lateral flanks, but only curved ones.
- The curvilinear profile of the lateral flanks is mathematically represented as a transcendental function, in which the parameters are the actual parameters of the thread: the diameter, pitch, and geometric parameters of the thread cutter: rake angle, half-profile angle, and inclination angle of its cutting edge.
- In case of using the known or scientifically justified values of the rake angles of thread-turning cutters up to 8–12°, the obtained flank profile of the thread becomes close to rectilinear, and the value of the thread half-profile angles can be within the tolerance field for angular deviation.
- As the value of the tool rake angle decreases to 4° and the threaded part diameter increases from 65 up to 117 (mm), the value of the predicted thread half-profile angle approaches the nominal value.
- In the case of using zero values of the geometric parameters of the thread-turning cutter, the convolute helicoid as part of the thread surface changes to an oblique closed helicoid (Archimedes' screw), and its profile contains a straight flank line.
- In the case of exactly zero values of the geometric parameters of the thread-turning cutter, namely the inclination angle of the edge and the rake angle, the transcendental expression describing the lateral thread profiles turns into a linear algebraic equation describing the profile of standard threads.

In the near future, it is planned to study the influence of lathe tool setting deviations on thread profile accuracy.

Author Contributions: Conceptualization, O.O.; methodology, O.O., V.K. and V.P.; software, O.O. and V.K.; validation, Y.K., M.B. and V.P.; formal analysis, V.K., S.B. and V.P.; investigation, O.O., C.B. and Y.K.; resources, C.B., S.B. and P.D.; data curation, C.B., M.B. and P.D.; writing—original draft preparation, O.O.; writing—review and editing, P.D. and S.B.; visualization, M.B. and V.P.; supervision, V.P.; project administration, P.D. and V.P.; funding acquisition, C.B., S.B. and M.B. All authors have read and agreed to the published version of the manuscript.

Funding: This research was funded by the Ministry of Education and Science of Ukraine, grant number PK 0124U000654.

Data Availability Statement: Data are contained within the article.

Acknowledgments: The team of authors express their gratitude to the reviewers for their valuable recommendations that have been taken into account to significantly improve the quality of this paper.

Conflicts of Interest: The authors declare no conflicts of interest. The funders had no role in the design of the study; in the collection, analyses, or interpretation of data; in the writing of the manuscript; or in the decision to publish the results.

References

1. Wang, H.; Huang, H.; Bi, W.; Ji, G.; Zhou, B.; Zhuo, L. Deep and ultra-deep oil and gas well drilling technologies: Progress and prospect. *Nat. Gas Ind. B* **2022**, *9*, 141–157. [CrossRef]
2. Sharmin, T.; Rodoshi Khan, N.; Md Saleh Akram; Ehsan, M.A. State-of-the-Art Review on Geothermal Energy Extraction, Utilization, and Improvement Strategies: Conventional, Hybridized, and Enhanced Geothermal Systems. *Int. J. Thermofluids* **2023**, *18*, 100323. [CrossRef]
3. Wu, B.; Zhang, K.; Meng, G.; Suo, X. Optimization of Recharge Schemes for Deep Excavation in the Confined Water-Rich Stratum. *Sustainability* **2023**, *15*, 5432. [CrossRef]
4. Chen, F.; Huo, Y.; Zhao, H.; Di, Q.; Wang, W.; Zhou, X.; Zhang, Y. The effect of axial tension and borehole curvature on torsion limit of drill string threaded connections. *Eng. Fail. Anal.* **2021**, *127*, 105555. [CrossRef]
5. *ISO 11961:2018*; International Standard. Petroleum and Natural Gas Industries—Steel Drill Pipe (MOD), 2nd ed. 1 November 2008. ISO: Geneva, Switzerland, 2008.
6. *GOST R 50278-92*; Drill Pipes with Weld-On Tool Joints. Specifications IS: Moscow, Russia, 1992. (In Russian)
7. Vlasiy, O.; Mazurenko, V.; Ropyak, L.; Rogal, O. Improving the aluminum drill pipes stability by optimizing the shape of protector thickening. *East. Eur. J. Enterp. Technol.* **2017**, *1*, 25–31. [CrossRef]
8. Bazaluk, O.; Slabyi, O.; Vekeryk, V.; Velychkovych, A.; Ropyak, L.; Lozynskyi, V. A technology of hydrocarbon fluid production intensification by productive stratum drainage zone reaming. *Energies* **2021**, *14*, 3514. [CrossRef]
9. Chudyk, I.; Velychkovych, A.; Grydzhuk, J. A Modeling of the Inertia Properties of a Drill String Section as a Continual Bent Rotating Rod. *SOCAR Proc.* **2021**, *2021*, 24–32. [CrossRef]
10. Prysyazhnyuk, P.; Molenda, M.; Romanyshyn, T.; Ropyak, L.; Romanyshyn, L.; Vytvytskyi, V. Development of a hardbanding material for drill pipes based on high-manganese steel reinforced with complex carbides. *Acta Montan. Slovaca* **2022**, *27*, 685–696.
11. Bembenek, M.; Prysyazhnyuk, P.; Shihab, T.; Machnik, R.; Ivanov, O.; Ropyak, L. Microstructure and Wear Characterization of the Fe-Mo-B-C—Based Hardfacing Alloys Deposited by Flux-Cored Arc Welding. *Materials* **2022**, *15*, 5074. [CrossRef]
12. Grydzhuk, J.S.; Dzhus, A.P.; Grydzhuk, J.S.; Dzhus, A.P.; Yurych, A.R.; Yurych, L.R.; Riznychuk, A.I.; Pylypaka, O.P. Approbation of the method for ensuring operational reliability and evaluating the residual life of drill string elements. In Proceedings of the 16th International Conference Monitoring of Geological Processes and Ecological Condition of the Environment, Monitoring 2022, Kyiv, Ukraine, 15–18 November 2022; EAGE: Amsterdam, The Netherlands, 2022; pp. 1–5.
13. Kopei, V.; Onysko, O.; Kusyi, Y.; Vriukalo, V.; Lukan, T. Investigation of the Influence of tapered Thread Pitch Deviation on the Drill-String Tool-Joint Fatigue Life. In *Lecture Notes in Networks and Systems, New Technologies, Development and Application V. NT 2022*; Karabegović, I., Kovačević, A., Mandžuka, S., Eds.; Springer: Cham, Switzerland, 2023; Volume 472, pp. 144–154.
14. Shatskyi, I.; Ropyak, L.; Velychkovych, A. Model of contact interaction in threaded joint equipped with spring-loaded collet. *Eng. Solid Mech.* **2020**, *8*, 301–312. [CrossRef]
15. Croccolo, D.; De Agostinis, M.; Fini, S.; Mele, M.; Olmi, G.; Scapecchi, C.; Tariq, M.H.B. Failure of Threaded Connections: A Literature Review. *Machines* **2023**, *11*, 212. [CrossRef]
16. Ropyak, L.Y.; Vytvytskyi, V.S.; Velychkovych, A.S.; Pryhorovska, T.O.; Shovkoplias, M.V. Study on grinding mode effect on external conical thread quality. *IOP Conf. Ser. Mater. Sci. Eng.* **2021**, *1018*, 012014. [CrossRef]
17. Wang, Y.; Qian, C.; Kong, L.; Zhou, Q.; Gong, J. Design Optimization for the Thin-Walled Joint Thread of a Coring Tool Used for Deep Boreholes. *Appl. Sci.* **2020**, *10*, 2669. [CrossRef]
18. Grydzhuk, J.; Chudyk, I.; Velychkovych, A.; Andrusyak, A. Analytical estimation of inertial properties of the curved rotating section in a drill string. *East. Eur. J. Enterp. Technol.* **2019**, *1*, 6–14. [CrossRef]

19. Pryhorovska, T.O.; Ropyak, L. Machining Error Influnce on Stress State of Conical Thread Joint Details. In Proceedings of the 8th International Conference on Advanced Optoelectronics and Lasers (CAOL 2019), Sozopol, Bulgaria, 6–8 September 2019; pp. 493–497.
20. Tutko, T.; Dubei, O.; Ropyak, L.; Vytvytskyi, V. Determination of Radial Displacement Coefficient for Designing of Thread Joint of Thin-Walled Shells. In *Lecture Notes in Mechanical Engineering, Advances in Design, Simulation and Manufacturing IV. DSMIE 2021*; Ivanov, V., Trojanowska, J., Pavlenko, I., Zajac, J., Peraković, D., Eds.; Springer: Cham, Switzerland, 2021; pp. 153–162.
21. Onysko, O.; Panchuk, V.; Kusyi, Y.; Odosii, Z.; Lukan, T. Impact of the Tool's Flank Clearance Angle on the Pitch Diameter Accuracy of the Tool-Joint Tapered Thread. In *Lecture Notes in Mechanical Engineering, Advances in Design, Simulation and Manufacturing V. DSMIE 2022*; Ivanov, V., Trojanowska, J., Pavlenko, I., Rauch, E., Peraković, D., Eds.; Springer: Cham, Switzerland, 2022; pp. 312–321.
22. Kopei, V.; Onysko, O.; Odosii, Z.; Pituley, L.; Goroshko, A. Investigation of the influence of tapered thread profile accuracy on the mechanical stress, fatigue safety factor and contact pressure. In *Lecture Notes in Networks and Systems, New Technologies, Development and Application IV. NT 2021*; Karabegović, I., Ed.; Springer: Cham, Switzerland, 2021; Volume 233, pp. 177–185.
23. Dubei, O.Y.; Tutko, T.F.; Ropyak, L.Y.; Shovkoplias, M.V. Development of Analytical Model of Threaded Connection of Tubular Parts of Chrome-Plated Metal Structures. *Metallofiz. Noveishie Tekhnol.* **2022**, *44*, 251–272. [CrossRef]
24. Rong, L.; Tie, Z.; Wu, X.J.; Wang, C.H. Crack closure effect on stress intensity factors of an axially and a circumferentially cracked cylindrical shell. *Int. J. Fract.* **2004**, *125*, 227–248.
25. Shats'kyi, I.P. Closure of a longitudinal crack in a shallow cylindrical shell in bending. *Mater. Sci.* **2005**, *41*, 186–191. [CrossRef]
26. Shatskii, I.P.; Makoviichuk, N.V. Effect of closure of collinear cracks on the stress-strain state and the limiting equilibrium of bent shallow shells. *J. Appl. Mech. Tech. Phys.* **2011**, *52*, 464–470. [CrossRef]
27. Adizova, A.; Abdieva, G.; Mavlanov, T. Computer modelling of dynamics of the thread in technological process. *J. Phys. Conf. Ser.* **2022**, *2373*, 022060. [CrossRef]
28. Saber, M.; Chouikhi, H. Finite Element Analyses of Bolted Joints Using Different Thread Modelling Techniques. *Teh. Vjesn.* **2022**, *30*, 178–184. [CrossRef]
29. Merticaru, V.; Nagît, G.; Dodun, O.; Merticaru, E.; Ripanu, M.I.; Mihalache, A.M.; Slatineanu, L. Influence of Machining Conditions on Micro-Geometric Accuracy Elements of Complex Helical Surfaces Generated by Thread Whirling. *Micromachines* **2022**, *13*, 1520. [CrossRef] [PubMed]
30. Bracken, P. Helicoidal Surfaces and Their Relationship to Bonnet Surfaces. *Adv. Pure Math.* **2017**, *7*, 31–40. [CrossRef]
31. Bazaluk, O.; Velychkovych, A.; Ropyak, L.; Pashechko, M.; Pryhorovska, T.; Lozynskyi, V. Influence of heavy weight drill pipe material and drill bit manufacturing errors on stress state of steel blades. *Energies* **2021**, *14*, 4198. [CrossRef]
32. Demirpolat, H.; Binali, R.; Patange, A.D.; Pardeshi, S.S.; Gnanasekaran, S. Comparison of Tool Wear, Surface Roughness, Cutting Forces, Tool Tip Temperature, and Chip Shape during Sustainable Turning of Bearing Steel. *Materials* **2023**, *16*, 4408. [CrossRef] [PubMed]
33. Sitarz, P.; Powałka, B. A new approach to improve noncircular turning process. *Int. J. Adv. Manuf. Technol.* **2019**, *104*, 3343–3360. [CrossRef]
34. Zhao, G.; Zhao, B.; Ding, W.; Xin, L.; Nian, Z.; Peng, J.; He, N.; Xu, J. Nontraditional energy-assisted mechanical machining of difficult-to-cut materials and components in aerospace community: A comparative analysis. *Int. J. Extrem. Manuf.* **2024**, *6*, 022007. [CrossRef]
35. Baizeaua, T.; Campocasso, S.; Fromentin, G.; Rossi, F.; Poulachon, G. Effect of rake angle on strain field during orthogonal cutting of hardened steel with c-BN tools. *Procedia CIPR* **2015**, *31*, 166–171. [CrossRef]
36. Litvin, F.; Gonzalez-Perez, I.; Yukishima, K.; Fuentes, A.; Hayasaka, K. Design, simulation of meshing, and contact stresses for an improved worm gear drive. *Mech. Mach. Theory* **2007**, *42*, 940–959. [CrossRef]
37. Kusyi, Y.; Stupnytskyy, V.; Onysko, O.; Dragašius, E. Optimization synthesis of technological parameters during manufacturing of the parts. *Eksploat. I Niezawodn.* **2022**, *24*, 655–667. [CrossRef]
38. Ivchenko, O.; Ivanov, V.; Trojanowska, J.; Zhyhylii, D.; Ciszak, O.; Zaloha, O.; Pavlenko, I.; Hladyshev, D. Method for an Effective Selection of Tools and Cutting Conditions during Precise Turning of Non-Alloy Quality Steel C45. *Materials* **2022**, *15*, 505. [CrossRef]
39. Petrakov, Y.; Danylchenko, M. A Time-Frequency Approach to Ensuring Stability of Machining by Turning. *East. Eur. J. Enterp. Technol.* **2022**, *6*, 85.
40. Pasternak, S.; Danylchenko, Y.M.; Storchak, M.; Okhrimenko, O.A. Gear Cutting with Disk-Shaped Milling Cutters. In *Advances in Gear Theory and Gear Cutting Tool Design*; Radzevich, S.P., Storchak, M., Eds.; Springer: Cham, Switzerland, 2022; pp. 151–179.
41. Danylchenko, Y.M.; Kryvosheia, A.V.; Melnyk, V.Y.; Tkach, P.M. Generalizing Structural Unified Model of the Synthesis of Links of Flat-Toothed Gearing Systems. In *Advances in Gear Theory and Gear Cutting Tool Design*; Radzevich, S.P., Storchak, M., Eds.; Springer: Cham, Switzerland, 2022; pp. 445–483.
42. Gu, W.; Li, C.; Miao, J.; Wang, P.; Chen, B. Wear Prediction Method of Differential Planetary Roller Screws Considering the Ambient Temperature Variations. *Appl. Sci.* **2023**, *13*, 10609. [CrossRef]
43. Yeh, S.-S.; Jiang, W.-J. Development of Pitch Cycle-Based Iterative Learning Contour Control for Thread Milling Operations in CNC Machine Tools. *Appl. Sci.* **2023**, *13*, 6447. [CrossRef]

44. Del Val, A.G.; Veiga, F.; Pereira, O.; De Lacalle, L.N.L. Threading Performance of Different Coatings for High Speed Steel Tapping. *Coatings* **2020**, *10*, 464. [CrossRef]
45. Del Val, A.G.; Veiga, F.; Suárez, A.; Arizmendi, M. Thread Quality Control in High-Speed Tapping Cycles. *J. Manuf. Mater. Process.* **2020**, *4*, 9. [CrossRef]
46. Li, X.; Wang, S.; Xu, K. Automatic Measurement of External Thread at the End of Sucker Rod Based on Machine Vision. *Sensors* **2022**, *22*, 8276. [CrossRef] [PubMed]
47. Li, K.; Jiang, L.; Chen, M. Experimental Study on the Influence of Cutting Parameters on Thread Precision of External Thread Turning. *MSF* **2013**, *770*, 7–12. [CrossRef]
48. Araujo, A.C.; Mello, G.M.; Cardoso, F.G. Thread milling as a manufacturing process for API threaded connection: Geometrical and cutting force analysis. *J. Manuf. Process.* **2015**, *18*, 75–83. [CrossRef]
49. Lin, E.-Y.; Chen, J.-C.; Lien, J.-J.J. Intelligent Tapping Machine: Tap Geometry Inspection. *Sensors* **2023**, *23*, 8005. [CrossRef]
50. Li, Z.; Fu, X.; Li, J.; Jiang, B.; Wang, F. Establishment of vibration wear model for turning large-pitch thread tools and its wear suppression method. *Int. J. Adv. Manuf. Technol.* **2020**, *109*, 857–876. [CrossRef]
51. Khoshdarregi, M.R.; Altintas, Y. Dynamics of Multipoint Thread Turning—Part I: General Formulation. *J. Manuf. Sci. Eng.* **2018**, *140*, 061003. [CrossRef]
52. Koleva, S.; Enchev, M.; Szecsi, T. Compensation of the deviations caused by mechanical deformations during machining of threads. *Procedia Manuf.* **2017**, *13*, 480–486. [CrossRef]
53. Khoshdarregi, M.R.; Altintas, Y. Generalized modeling of chip geometry and cutting forces in multi-point thread turning. *Int. J. Mach. Tools Manuf.* **2015**, *98*, 21–32. [CrossRef]
54. Khani, S.; Shahabi, H.S.; Razfar, M.R.; Farahnakian, M. Improvement of thread turning process using micro-hole textured solid-lubricant embedded tools. *Proc. Inst. Mech. Eng. Part. B J. Eng. Manuf.* **2021**, *235*, 1727–1738. [CrossRef]
55. Khoshdarregi, M.R.; Altintas, Y. Dynamics of Multipoint Thread Turning—Part II: Application to Thin-Walled Oil Pipes. *J. Manuf. Sci. Eng.* **2018**, *140*, 041016. [CrossRef]
56. Krawczyk, B.; Szablewski, P.; Mendak, M.; Gapiński, B.; Smak, K.; Legutko, S.; Wieczorowski, M.; Miko, E. Surface Topography Description of Threads Made with Turning on Inconel 718 Shafts. *Materials* **2022**, *16*, 80. [CrossRef] [PubMed]
57. Neshta, A.; Kryvoruchko, D.; Hatala, M.; Ivanov, V.; Botko, F.; Radchenko, S.; Mital, D. Technological Assurance of High-Efficiency Machining of Internal Rope Threads on Computer Numerical Control Milling Machines. *J. Manuf. Sci. Eng.* **2018**, *140*, 071012. [CrossRef]
58. He, Q.; Jiang, Y.; Jing, X.; Jiang, Y.; Zhou, H.; Fu, B. Research and Optimization of Process Parameters for Internal Thread Forming Based on Numerical Simulation and Experimental Analysis. *Materials* **2022**, *15*, 3160. [CrossRef]
59. Chen, T.-C.; Lian, J.-J.; Wang, C.-C. Analysis of Micro-Machining Process for External Thread of Micro Round Tube. *Materials* **2021**, *14*, 4327. [CrossRef]
60. Zanger, F.; Sellmeier, V.; Klose, J.; Bartkowiak, M.; Schulze, V. Comparison of modeling methods to determine cutting tool profile for conventional and synchronized whirling. *Procedia CIPR* **2017**, *58*, 222–227. [CrossRef]
61. Onysko, O.; Panchuk, V.; Kopei, V.; Pituley, L.; Lukan, T. Influence of Back Rake Angle of a Threading Cutter on the Drill-String Tool-Joint Pitch Diameter. In *Lecture Notes in Mechanical Engineering, Grabchenko's International Conference on Advanced Manufacturing Processes (InterPartner 2022)*; Tonkonogyi, V., Ivanov, V., Eds.; Springer: Cham, Switzerland, 2023; pp. 200–210.
62. Kacalak, W.; Majewski, M.; Budniak, Z.; Ponomarenkow, J. Worm Gear Drives with Improved Kinematic Accuracy. *Materials* **2021**, *14*, 7825. [CrossRef]
63. *API SREC 7-2*; Specification for Threading and Gauging of Rotary Shouldered Thread Connection, Second Edition. API: Washington, DC, USA, 2020.
64. Sandvik Coromant. Tread Turning Tools. Available online: https://www.sandvik.coromant.com/en-us/tools/threading-tools/thread-turning-tools (accessed on 11 March 2024).
65. Costa, C.E.; Polli, M.L. Effects of the infeed method on thread turning of AISI 304L stainless steel. *J. Braz. Soc. Mech. Sci. Eng.* **2021**, *43*, 253. [CrossRef]
66. Günay, M. Investigation of the Effects on Screw Thread of Infeed Angle during External Threading. *Gazi Univ. J. Sci.* **2011**, *24*, 153–160.
67. An, Q.L.; Guo, G.G.; Zheng, X.H.; Chen, M.; Liu, G.; Zhang, Y.S. Experimental Study on Cutting Characteristics for Buttress Thread Turning of 13%Cr Stainless Steel. *Key Eng. Mater.* **2010**, *443*, 262–267. [CrossRef]
68. Onysko, O.; Kopei, V.; Vytvytskyi, V.; Vriukalo, V.; Lukan, T. Calculation of the Accuracy of the Drill-String NC13 Thread Profile Turned from Difficult-to-Machine Steel. In *Lecture Notes in Mechanical Engineering; Advanced Manufacturing Processes V. InterPartner 2023*; Tonkonogyi, V., Ivanov, V., Eds.; Springer: Cham, Switzerland, 2024; pp. 182–192. [CrossRef]
69. Workpiece Material Group. Available online: https://5wyuco84ao39w9tsgkkmnmx.blob.core.windows.net/cms/WMG_summary.pdf (accessed on 19 April 2024).
70. 630 (1.4542) Stainless Steel. Available online: https://bircelik.com/en/category/630-1-4542 (accessed on 19 April 2024).
71. Onysko, O.; Medvid, I.; Panchuk, V.; Rodic, V.; Barz, C. Geometric Modeling of Lathe Cutters for Turning High-Precision Stainless Steel Tapered Threads. In *Lecture Notes in Mechanical Engineering, Advances in Design, Simulation and Manufacturing IV. DSMIE 2021*; Ivanov, V., Trojanowska, J., Pavlenko, I., Zajac, J., Peraković, D., Eds.; Springer: Cham, Switzerland, 2021; pp. 472–480.

72. Caltaru, M.; Ripeanu, R.; Badicioiu, R.; Zisopol, D.R. Experimental Researches to Establish the Optimum Hardbanding Technology and Materials of the Heavy Weight Drill Pipe. *MATEC Web Conf.* **2020**, *318*, 01017. [CrossRef]
73. JFE-TC. UHP^{TM}-15CR-125. Available online: https://jfetc.com/product/uhp-15cr/ (accessed on 19 April 2024).
74. Medvid, I.; Onysko, O.; Panchuk, V.; Pituley, L.; Schuliar, I. Kinematics of the Tapered Thread Machining by Lathe: Analytical Study. In *Lecture Notes in Mechanical Engineering, Advanced Manufacturing Processes II (InterPartner 2020)*; Tonkonogyi, V., Ivanov, V., Trojanowska, J., Oborskyi, G., Grabchenko, A., Pavlenko, I., Edl, M., Kuric, I., Dasic, P., Eds.; Springer: Cham, Switzerland, 2021; pp. 555–565.
75. Slătineanu, L.; Radovanovic, M.; Coteață, M.; Beșliu, I.; Dodun, O.; Coman, I.; Olaru, S.-C. Requirements in designing a device for experimental investigation of threading accuracy. *MATEC Web Conf.* **2017**, *112*, 01005. [CrossRef]
76. Boral, P.; Gołębski, R. Technology of Manufacturing of ZC Cylindrical Worm. *Materials* **2022**, *15*, 6412. [CrossRef]
77. Andrianto, M.; Wu, Y.R.; Arifin, A. Mathematical modeling on a novel manufacturing method for roller-gear cams using a whirl-machining process. *Int. J. Adv. Manuf. Technol.* **2023**, *125*, 5015–5029. [CrossRef]
78. Kacalak, W.; Szafraniec, F. Analiza kształtu i położenia strefy obróbki w procesie szlifowania powierzchni śrubowych ślimaków stożkowych. *Mechanik* **2015**, *8–9*, 159–163.
79. Onysko, O.; Kopei, V.; Kusyj, Y.; Kornuta, O.; Schuliar, I. Turning of NC10 Threads for Drill Pipes: Theoretical Study of the Designed Profile. In *Lecture Notes in Mechanical Engineering, Advances in Design, Simulation and Manufacturing VI. DSMIE 2023*; Ivanov, V., Trojanowska, J., Pavlenko, I., Rauch, E., Piteľ, J., Eds.; Springer: Cham, Switzerland, 2023; pp. 356–366.
80. Onysko, O.R. The Theoretical Foundations of the Threading Tool Bits Designing for Lathe Machining of the Drill String Tool-Joint Connectors with the Increased Operating Characteristics. Ph.D. Thesis, Odessa National Polytechnic University, Odessa, Ukraine, 2020. (In Ukrainian)
81. Fromentin, G.; Poulachon, G. Geometrical analysis of thread milling—Part 1: Evaluation of tool angles. *Int. J. Adv. Manuf. Technol.* **2010**, *49*, 73–80. [CrossRef]
82. Fu, X.; Li, K.; Li, Z.; Wang, X. A SVM-based design method for cutting edge profile stability of large-pitch thread turning tool considering vibration. *Int. J. Adv. Manuf. Technol.* **2023**, *125*, 4529–4547. [CrossRef]